International Journal of Climatology

International Journal of Climatology | RMetS

RESEARCH ARTICLE OPEN ACCESS

Assessment of Anticipated Changes in Extreme Temperature and Precipitation Under 1.5°C and 2°C Warming Over the Mississippi River Basin

Atanas Dommo[1,2,3] | Zachary Leasor[1,4] | Anthony Lupo[1,4] | Sherry Hunt[5] | Noel Aloysius[1,2,4,6]

[1]School of Natural Resources, University of Missouri, Columbia, Missouri, USA | [2]Department of Chemical and Biomedical Engineering, University of Missouri, Columbia, Missouri, USA | [3]National Advanced School of Engineering, University of Yaounde I, Yaounde, Cameroon | [4]Missouri Climate Center, University of Missouri, Columbia, Missouri, USA | [5]Agroclimate and Hydraulics Engineering Research Unit, United States Department of Agriculture—Agricultural Research Service, Oklahoma and Central Plains Agricultural Research Center, Stillwater, Oklahoma, USA | [6]Missouri Water Center, University of Missouri, Columbia, Missouri, USA

Correspondence: Atanas Dommo (ad7gb@missouri.edu)

Received: 18 April 2025 | **Revised:** 19 September 2025 | **Accepted:** 22 September 2025

Funding: This work was supported by the U.S. Department of Agriculture.

Keywords: extreme precipitation | Mississippi River Basin | projections | uncertainty

ABSTRACT

Extreme precipitation and temperature have large socioeconomic and human health impacts. This study aims to analyse the projected changes of extreme precipitation and temperature indices at 1.5°C and 2°C of warming over the Mississippi River Basin (MRB) under Shared Socio-economic pathways (SSP) 2-4.5 and SSP5-8.5. We used a technique named bias correction constructed analogues with quantiles mapping reordering (BCCAQ) to downscale daily precipitation, minimum and maximum temperature from a set of 12 Coupled Models Intercomparison Project phase 6 (CMIP6) over MRB. The changes in extreme precipitation and temperature indices such as very heavy rainfall (R95p), warm days (TX90p), and warm spell duration (WSDI) are sensitive to warming targets and emission scenarios. Results indicate that both warming targets are expected to exacerbate R95p whilst intensifying extreme precipitation and temperature as a whole except for cumulative wet days (CWD) (many parts of MRB are experiencing reduced CWD at both warming targets and scenarios). However, the rainfall intensity (SDII) is more reduced under SSP5-8.5 compared to SSP2-4.5 with an additional 0.5°C highlighting the sensitivity of SDII to the emission scenario. An additional 0.5°C (from 1.5°C to 2°C) climate warming is expected to: (1) increase TX90p and WSDI by 50% under SSP2-4.5 and nearly 100% under SSP5-8.5 over much of the MRB subregions, (2) reduce extreme precipitation in the centre of the MRB. Uncertainty superimposes on the magnitude of changes with more than 75% contribution from internal climate variability to total variance, nearly 20% from climate models, and marginal contribution from climate scenarios. The predominance of natural climate variability underscores a decreased predictability in future extreme precipitation and extreme temperature due to anthropogenic forcings, particularly at the regional scale. So, a deep understanding of what drives climate and its variability on a local and regional scale is critical for future generations of climate models and climate projections assessment. However, climate warming will pose serious challenges to water availability over the MRB, with consequences for agriculture, crop yields, and ecosystems.

1 | Introduction

There is international agreement that the 2°C surface temperature warming above preindustrial level carries with it an excessive risk for human activities, and that there is a need to target global warming below 1.5°C (Rogelj et al. 2015). According to the International Panel on Climate Changes (IPCC 2022) Sixth Assessment Report (SAR), continuous warming is already affecting each inhabited region across the world. If no coercive mitigation plan is implemented by the main international players, the global mean temperature will exceed the 1.5°C set by 2015 Paris agreement in the next two decades (Masson-Delmotte et al. 2021), with a consequent increase in the number of extreme weather events, such as flooding, droughts and heatwaves.

Over the US, many studies (Peterson et al. 2013; Akinsanola et al. 2020; Anderson et al. 2010, 2015; Dommo et al. 2024) have underscored the increases of extreme precipitation and temperature over the recent past decades. Expectations from projected changes of precipitation (Zhao et al. 2023; Akinsanola et al. 2020; Jong et al. 2023) and temperature (Aerenson et al. 2018) related extreme indices point to an overall increase owing to climate warming. Although previous studies provided valuable insights into the projected extreme temperature and precipitation indices, few of them have considered the different Global Warming Levels (GWLs) which are crucial for assessing the impact of limiting global warming below 1.5°C compared to 2°C. In addition, none of them have assessed the uncertainty associated with projected changes which is important for resources allocation and long-term mitigation plan. Then, the US lacks a significant assessment of projected climates' extreme indices considering GWLs and the associated uncertainties. Assessing changes under GWLs and their uncertainty is crucial to avoid allocating resources or mitigation policies by targeting areas which are not of the greatest need. The 1 September 2021 record breaking rainfall over the northeast United States inundated densely populated areas and caused more than $20 billion in losses (Smith et al. 2023). So, there is increasing concern about whether the existing infrastructure is at risk due to a changing climate.

On a regional scale, detecting and projecting changes in precipitation remain a challenge and uncertain (Kharin et al. 2013; Pfahl et al. 2017; Xie et al. 2015) partly due to limitations coming from coarse gridded global climate projections. However, even if the concern regarding model resolution were resolved, other sources of uncertainties that generally account for future projection are (Hawkins and Sutton 2009, 2010): (1) internal variability (2), model uncertainty and (3) scenario uncertainty. The latter uncertainty generally occurs when assessing future projections from climate scenarios. Assessing uncertainty in projected extreme indices can help avoid large costs associated with insufficient or unnecessarily rigorous adaptation (Eisenack and Paschen 2022). Regions like the Mississippi river basin (MRB) are highly vulnerable to climate fluctuations due to its significant agricultural and livestock production (Foley et al. 2004). The present study investigates the benefits of mitigating the average temperature to 2°C or less by computing a set of extremes precipitation and temperature indices and investigating how they change across two warming scenarios and to what extent there can be confidence in the changes in order to inform research and mitigation choices, since climates extreme have more impact on human and natural ecosystems.

Therefore, in this study, we seek to answer the questions: (1) how do precipitation and temperature related extreme indices change over the MRB under 1.5°C and 2°C global warming scenario? (2) what are the magnitudes of the uncertainties associated with the projected changes? (3) Could the simulated changes be associated with anthropogenic climate forcings? To this end, we utilise a set of 12 high-resolution downscaled climate models under Shared Socio-Economic Pathways (SSPs) 2-4.5 and SSP5-8.5 to assess the projected changes of four precipitation and five temperature related indices (Table 1) from the Expert Team on Climate Change Detection and Indices (ETCCDI) under 1.5°C and 2°C global warming over the MRB and its corresponding sub-basins. This suite of indices gives a rich picture of climates relevant to different sub-basins over MRB. The high-resolution downscaled data used in this study are the output of bias correction constructed analogues with quantiles mapping reordering (BCCAQ) which has been shown to efficiently removing biases and reproducing event scale spatial gradients. In addition, for precipitation, the selected indices address both minimum and maximum temperature behaviour. The uncertainties are also evaluated following the methodology described below. The manuscript is organised as follows: Section 2 represents the data used; Section 3 provides a description of the different methods used in this work. Results are presented in Section 4. The discussion of our results is provided in Section 5 followed by the conclusion in Section 6.

2 | Data and Study Area

2.1 | Data

2.1.1 | CMIP6 Simulations

The modelled daily dataset (precipitation, near surface average, minimum and maximum temperature), used in this study is from the Coupled Model Intercomparison Project Phase 6 (CMIP6, Eyring et al. 2016). These data are obtained from the outputs of 12 CMIP6 models spanning from 1950 to 2099 (see Table S1 for spatial resolution, institutions, model names, and variables). CMIP6 represents an updated version of previous iterations such as CMIP3 (Meehl et al. 2007) and CMIP5 (Taylor et al. 2012) with changes in model configuration including model resolution, physical processes, and atmospheric chemistry treatment. This study assesses the changes in four extreme precipitation and five temperature extreme indices under 1.5°C and 2°C global warming above preindustrial level, using two shared socio economic scenarios (O'Neill et al. 2016): (1) the middle of the road scenario (hereafter, SSP2-4.5) considered as the moderate scenario which assumes that climate protection measures are being taken, and (2) the fossil fuel development scenario (hereafter, SSP5-8.5) which is the worst-case climate scenario based on enhanced global economic and high percentage of coal and energy-intensive lifestyle worldwide.

2.1.2 | Observational Dataset

The daily dataset with 0.25° × 0.25° spatial resolution for the period 1950–2010 provided by Princeton University—Department of Civil and Environment Engineering (https://rda.ucar.edu/datasets/d314000/) was used to run the bias correction

TABLE 1 | List of temperature and precipitation indices used in this study.

Indices	Name	Definition	Unit
R20mm	Number of very heavy precipitation	Let RR_{ij} be the daily precipitation amount on day i in period j. Count the number of days where $RR_{ij} \geq 20$ mm	days
CWD	Cumulative wet or wet spell	Maximum number of days with precipitation ≥ 1 mm in a given period	days
SDII	Simple daily intensity index	Average rainfall from wet days. Let RRwj be the daily rainfall amount on wet-day, PRCP ≥ 1 mm in period j. If W represents number of wet days in j, then: $SDII_j$ is the total precipitation of wet for the period j divided by the number of wet days	mm/day
R95p	Very wet days total precipitation	Annual total PRCP when RR > 95th percentile. Let RR_{wj} be the daily precipitation amount on a wet day w (RR = 1.0 mm) in period i and let RR_{wn} 95 be the 95th percentile of precipitation on wet days in the reference period. If W represents the number of wet days in the period, then: $R95_p = \sum_{w=1}^{W} where\ RR_{wj} > RR_{wn}95$	mm
ETR	Extreme temperature range	Let TXx be the daily maximum temperature in month k and TNn the daily minimum temperature in month k. The extreme temperature range each month is then: $ETR_k = TXx_k - TNn_k$	°C
TXx	Maximum value of daily maximum temperature	Let TXx be the daily maximum temperatures in month k, period j. The maximum daily maximum temperature each month is then $TXx_{kj} = \max\left(TXx_{kj}\right)$	°C
TNn	Minimum value of daily minimum temperature	Let TNn be the daily minimum temperatures in month k, period j. The minimum daily minimum temperature each month is then $TNn_{kj} = \min\left(TNn_{kj}\right)$	°C
TX90p	Warm days	Number of days when TX > 90th percentile: Let TX_{ij} be the daily maximum temperature on day i in period j and let TX 90 be the 90th percentile for the given period. Count the number of days where $TX_{ij} > TX90$	days
WSDI	Warm spell duration	Annual count of days with at least 6 consecutive days when TX > 90th percentile: Let TX_{ij} be the daily maximum temperature on day i in period j and let TX_{in} 90 be the calendar day 90th percentile centred on a 5-day window for the period. Then the number of days per period is summed where, in intervals of at least 6 consecutive days: $TX_{ij} > TX_{in}$ 90	days

constructed analogues with quantiles mapping reordering. It is a global meteorological forcing dataset for land surface modelling and can be used to drive models (Sheffield et al. 2006). The dataset is a combination of National Centres for Environmental Predictions/National Centre for Atmospheric Research (NCEP/NCAR, Sheffield et al. 2006) reanalysis with global observation-based datasets. Daily minimum and maximum temperature, as well as daily precipitation from the period 1948–2010 can be retrieved from Research Data Archive (last access 12 August 2025, https://rda.ucar.edu/datasets/d314000/).

2.2 | Study Area

In this study, we focused on the MRB (Figure 1). It drains the fourth-largest river in the world, covering almost 41% of the conterminous US and encompasses 31 states (Muller and Schaetzl 1998). Economically, MRB is of national importance because of its potential in terms of hydroelectric power generation, agricultural and food productivity (Foley et al. 2004), transportation, and services. The river is joined by many other rivers and forms six main sub-basins such as: Missouri River basin (MO), Arkansas River basin (Ark), Upper MRB (UM), L MRB (LM), Ohio River basin (Ohio), and Tennessee River Basin (Ten). A recent study (Dommo et al. 2024) highlighted a decreasing trend in extreme precipitation over the MRB, such as heavy and very heavy precipitation found mostly in Ohio, LM, UM, Ten, and Ark, where the temperature components (mean, minimum, and maximum) are significantly increasing in concert with a warming climate. In addition to surface elevation and large-scale atmospheric and oceanic circulation (Dommo et al. 2024), extreme precipitation over the MRB is driven by moisture flux from the Gulf of Mexico. This intense moisture flux contributes to approximately 94% of the total precipitation (Bishop et al. 2019) over the Gulf of Mexico.

3 | Materials and Methods

3.1 | Bias Correction and Downscaling Technique

To make the simulation useful for an impact study at the local and regional level, we utilised an approach referred to as bias correction constructed analogues with quantiles

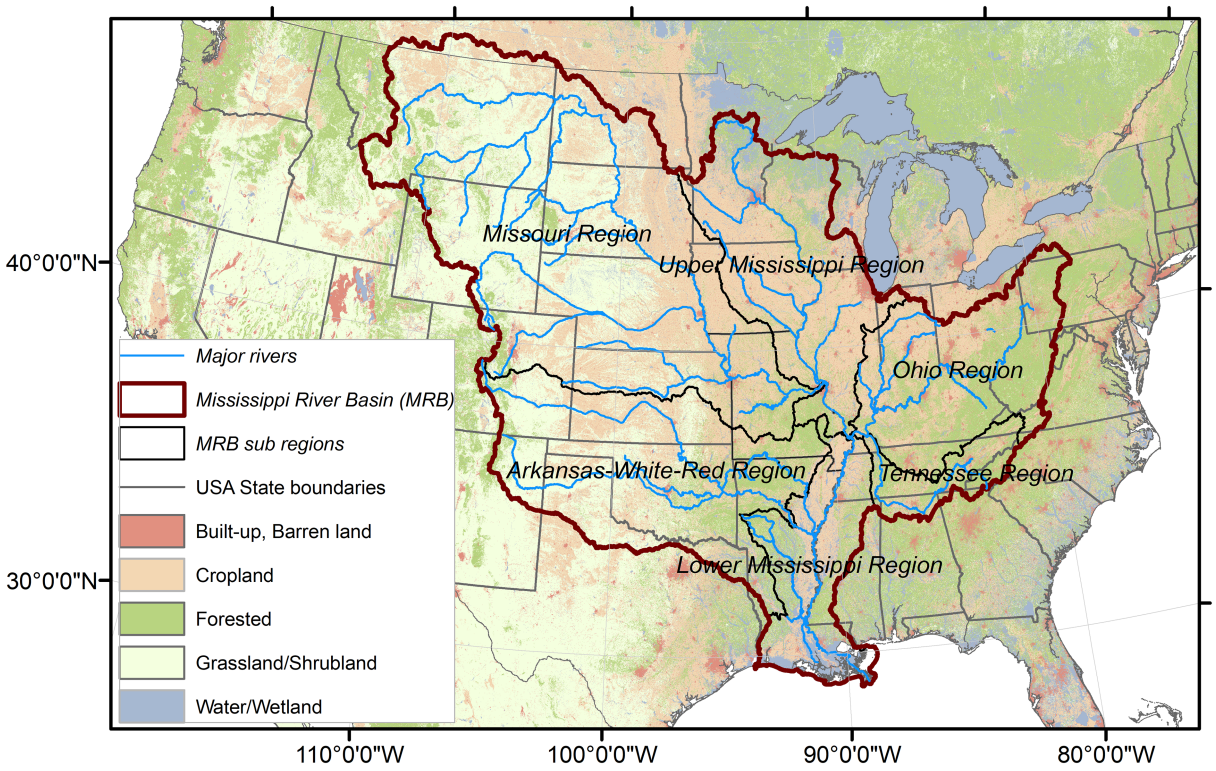

FIGURE 1 | Study area—the Mississippi River Basin and sub region boundaries are shown. The background map shows major land cover types. The sub regions denoted are Ark—Arkansas-White-Red River basin, LM—Lower Mississippi river basin, MO—Missouri river basin, Ohio—Ohio river basin, Ten—Tennessee river basin, and UM—Upper Mississippi river basin, respectively. [Colour figure can be viewed at wileyonlinelibrary.com]

mapping reordering (BCCAQ) to downscale the coarse resolution climate models to a finer resolution (Rettie et al. 2023a; Gebrechorkos et al. 2023; Werner and Cannon 2016). This technique has shown superior performance in removing bias from GCMs and reproducing extreme events (Gebrechorkos et al. 2023; Werner and Cannon 2016). BCCAQ is a hybrid downscaling method which combines bias Correction Climate Imprint (BCCI—Hunter and Meentemeyer 2005) and bias Correction Constructed Analogs (BCCA—Maurer et al. 2010). During the downscaling process, the BCCI interpolates the coarse resolution climate model to finer resolution using Quantile Delta Mapping (QDM—Cannon et al. 2015), whereas BCCA performs the quantile delta mapping between the GCMs and the spatially aggregated reference dataset to GCM resolution, and the relationship between the GCMs and the reference dataset is used to get the final bias corrected model data. It is worth noting that the BCCI and BCCA analyses are performed independently during the downscaling process, and the BCCAQ combines the outputs. For the Climate Imprint (CI) process, the raw GCM anomalies are interpolated firstly to the fine spatial resolution of the observation data. The anomaly for each day of the year is calculated by subtracting from the modelled daily value the corresponding monthly climatological value for that day. Secondly, for each day of the year, the monthly climatology derived from monthly observational data is added to the corresponding daily anomaly of the interpolated raw GCM daily anomaly for each grid cell. Thirdly, the QDM is used to bias correct the interpolated raw data obtained from the previous step. More details about the implementation of QDM are provided by Cannon et al. (2015) and Rettie et al. (2023b). Overall, BCCI prepares data for the next step by applying quantile mapping as a post-processing step to interpolate the fine scale outputs from CI. The Constructed Analogue (CA) steps include (1) aggregating the finer scale observed data to the GCM grid, (2) bias correcting raw GCM using QDM, (3) searching for a subset of analogue of the GCM weather pattern with the target pattern, and (4) determining a regression coefficient between the analogue and the target pattern to linearly combine the bias corrected CI outputs, creating a spatially high resolution downscaled data. A schematic process and the detailed steps for the BCCAQ can be found in Rettie et al. (2023a).

3.2 | Definition of the Time Reaching 1.5°C and 2°C Global Warming

According to the Paris Agreement, the 1.5°C and 2°C global warming thresholds are relative to the preindustrial period (Shi et al. 2018). In this study, the +1.5°C (+2°C) period is defined as the time when the 30-year running mean of the global mean temperature reaches +1.5°C (+2°C) compared to the preindustrial period following the methodology defined by Vautard et al. (2014). In this study, we considered the period 1971–2000 as the baseline period. However, based on observed surface temperature (NASA-Goddard Institute for Space Studies GISS Surface Temperature Analysis) (Hansen et al. 2010), we estimate a climate warming of around 0.46°C from the preindustrial period relative to the baseline period. Thus, for each CMIP6 model, the +1.5°C (+2°C) period is the year when the 30-year moving average of the global

mean temperature first reaches +1.04°C (+1.54°C) relative to the baseline period 1971–2000. Table S2 shows the crossing time at which each model reaches 1.5°C and 2°C global warming under each scenario (SSP2-4.5 and SSP5-8.5).

3.3 | Sources of Uncertainties in the Projected Climate Extremes

Usually, there are three types of uncertainty in climate projections, namely: (1) model uncertainties due to different projection produced by different models, (2) scenario uncertainty, which is related to radiative forcing considered for projection and (3) the internal variability which is the expression of the fluctuation in a long-term trend in each projection. Following the methodology proposed by Hawkins and Sutton (2009, 2010), we evaluated the uncertainty estimate in temperature and precipitation related indices (Table 1) for the period 2015–2099. Here the decomposition of uncertainty is computed based on the changes of climate extreme indices, considering the period 1971–2000 as the baseline period. In this study, the changes in precipitation indices are expressed as percentage following Equation (1)

$$\Delta Z(s,m,t)_{id} = 100 \times \left(\frac{I(s,m,t)_{id}}{\frac{1}{30} \times \sum_{t=1971}^{2000} I(s,m,t)_{id}} - 1 \right) \quad (1)$$

and the change in temperature is expressed as follows:

$$\Delta Z(s,m,t)_{id} = I(s,m,t)_{id} - \frac{1}{30} \times \sum_{t=1971}^{2000} I(s,m,t)_{id} \quad (2)$$

where $\Delta Z(s,m,t)_{id}$ is the changes in extreme indices $I(s,m,t)_{id}$ relative to the period 1971–2000. $s = 1, \ldots, N_s$, $m = 1, \ldots, N_m$, and $t = 1, \ldots, N_t$ refer to the number of SSPs, GCMs and years respectively. Here N_s, N_m and N_t are the number of the SSP, GCM and time length respectively. To assess the three different types of uncertainty cited above, the smooth mean changes of the indices for all GCMs and SSPs is divided into changing signal and the residual by fitting fourth order and second order polynomial regression to precipitation and temperature related indices respectively (Hawkins and Sutton 2009). The changes can be written as:

$$\Delta Z(s,m,t)_{id} = i(s,m,t) + \epsilon(s,m,t) \quad (3)$$

here $i(s,m,t)$ and $\epsilon(s,m,t)$ are the mean changes and residual respectively after fitting the fourth order and two order polynomial regression on precipitation and temperatures indices respectively. The total uncertainty can be quantified as follows:

$$T(t) = S(t) + M(t) + V \quad (4)$$

where $S(t)$, $M(t)$, and V are respectively the scenario uncertainty, the model uncertainty and the internal variability (see Supporting Information for details steps on how each uncertainty is separated and quantified).

3.4 | Signal to Noise Ratio

The signal to noise ratio (S/N) is evaluated to quantify the influence of uncertainties on changes in projected climates extreme. It can be expressed as follows:

$$S/N(t) = \frac{\bar{i}(t)}{1.65 \times \sqrt{T(t)}} \quad (5)$$

where $\bar{i}(t)$ denotes the average of the changes over all models and scenarios. A larger S/N underscores that the changes in projected climates extreme dominates the total uncertainty. In the same vein, a small S/N (less than unit is absolute value) indicates that the projected changes should be taken with caution since the uncertainty dominates the changing signal and thus do not provide suitable information for decision making. In this study we evaluated the S/N for all the six sub-basins over the MRB.

3.5 | Models' Evaluation

We evaluated the BCCAQ in simulating the spatial pattern and the amplitude of the extreme temperature and precipitation indices over the period 1971–2000 against the observational data described in Section 2.1.2. The evaluation metrics, such as Root Mean Square Error (RMSE), Pearson Correlation Coefficient (PCC), and mean bias error (MBE) (see Supporting Information for details), are also used to evaluate the ability of BCCAQ in reproducing the extreme precipitation and temperature related indices. Compared to raw climate models, the ensemble mean of the downscaled models can capture well the spatial pattern of the precipitation and temperature related indices (Figures S1 and S2). The evaluation metrics (RMSE, PCC, and MBE) before and after downscaling are presented in Figures S3–S6. The RMSE and MBE amongst precipitation indices are reduced considerably after downscaling and fall below units, particularly for R20mm and CWD (Figure S4), implying a good performance of BCCAQ in simulating the heavy precipitation and CWD. Similarly, the correlation between indices after downscaling is greater than 0.8. Although BCCAQ can simulate precipitation indices, bias still persists after downscaling, particularly for SDII and R95p (Figure S4); however, the amplitude of biases is reduced compared to bias before downscaling, where models overestimate SDII over the MRB. Overall, for SDII and R95p, BCCAQ provides significant improvement over the Missouri region compared to the lower Mississippi, Ohio, and Tennessee region. Regarding the temperature related indices, the RMSE is strongly reduced after downscaling (Figure S6) for all the indices compared to RMSE before downscaling (Figure S5). The correlation coefficients are improved significantly, particularly for TX90p and WSDI. The amplitude of MBE is also reduced significantly after the downscaling, except for TX90p, where a slight overestimation by a factor of 1.8 over the MRB is noticeable (Figure S6). Similarly, overestimated TXx in the northern Missouri region in raw models turns into underestimation after downscaling, suggesting that the used bias corrected method may also contribute to uncertainties in projected climate indices. Overall, the results from the bias correction method show that BCCAQ is able to capture the spatial pattern and considerably reduce the biases in precipitation and temperature related indices.

4 | Results

4.1 | Changes in Precipitation Extreme

We start by analysing the change in daily precipitation at GWL1.5 and GWL2 (Figure S7) over the MRB. Under ssp2-4.5 (Figure S7a,b), the daily precipitation increases on average by 137% (141%) at GWL1.5 (GWL2) relative to the period 1971–2000. Likewise, daily precipitation increases on average by 139% (141%) at GWL1.5 (GWL2) under SSP5-8.5 (Figure S7d,e). With an additional 0.5°C (from 1.5°C to 2°C) warming, daily precipitation increases on average by 4% and 2% under SSP2-4.5 and SSP5-8.5 respectively. Regionally, the Arkansas region will experience the highest rate of increased daily rainfall under SSP2-4.5 (SSP5-8.5), followed by the Missouri region and Upper Mississippi (Table 2). However, in terms of intensity, the Lower and Upper Mississippi, Southeastern part of Arkansas, and Tennessee will experience the highest increased daily rainfall ranging from 1.8 to 2.4 mm/day (Figure S8). Over Arkansas, increased daily precipitation could be associated with high elevated areas (Figure 1). With an additional 0.5°C warming relative to GWL1.5, increased rainfall is projected to occur over the entire MRB under SSP2-4.5, except over southwest Missouri and part of the Arkansas region where reduced daily precipitation is observed. Under SSP5-8.5, an additional 0.5°C warming projects to increase daily rainfall over the northern Missouri region, Ohio, and Tennessee region (Figure S7f). However, compared to SSP2-4.5 (Figure S7c), reduced daily rainfall with an additional 0.5°C extends to the Lower and Upper Mississippi, Arkansas, and southern Missouri region under SSP5-8.5 (Figure S7f). The difference between the changes in both scenarios (SSP2-4.5 and SSP5-8.5) shows moderate increased daily precipitation at GWL1.5 (Figure S7g); however, reduced daily precipitation is enhanced over almost the entire MRB at GWL2 (Figure S7h,i), particularly over the Missouri region, Arkansas, and Upper Mississippi.

Under SSP5-8.5 (Figure 2), a regional mean increase of SDII by 3.45% and 4.65% is associated with an increased heavy precipitation (R20mm) by 3.79% and 5.23% at GWL1.5 and GWL2 respectively. This implies an average increase of SDII and heavy rainfall by 1.14% and 1.37% respectively with an additional warming of 0.5°C. The northern Missouri region encompassing Montana, North and South Dakota, Wyoming will experience about 12% increased heavy rainfall with additional 0.5°C climate warming associated with an additional 4%–6% increased SDII. However, decreased heavy precipitation is observed over the Southwestern part and centre Missouri region as the SDII also decreases. Over the lower Mississippi (Ohio river basin), an average decreased (increased) heavy precipitation associated with increased SDII is more pronounced at GWL1.5 compared to GWL2. The regional differences in the changes for both global warming levels show that heavy rainfall is projected to be more frequent over the Ohio river basin with an increase of about 26% (20%) at GWL2 (GWL1.5) leading to an increase of up to 12% with an extra warming of 0.5°C. However, heavy precipitation events are likely to decrease by 6% over the Lower Mississippi, Centre Missouri and Arkansas Region at GWL2 relative to GWL1.5. The average regional increase of CWD is about 1.61% and 1.563% at GWL1.5 and GWL2 respectively. This implies an overall decrease in consecutive wet days with a warm climate over the MRB. The spatial variability shows that an increased CWD of about 6% is observed in south and northeast MRB at both GWL1.5 and GWL2. Decreased CWD is mostly observed at the north Missouri river basin encompassing Montana and Wyoming at GWL1.5. Overall, a decreased CWD is observed almost everywhere in the MRB with an additional warming of 0.5°C. Likewise, R95p is projected to increase by 14% and 16% on average at GWL1.5 and GWL2 respectively. The spatial variability shows an increase of R95p almost everywhere in the MRB at both warming levels, except in the western border of Arkansas region where decreased R95p by 8% is noticeable. The spatial variability exhibit that the Ohio river basin will experience increased R95p as the warming goes up. This exposes the Ohio river basin to natural disasters such as flooding as a response to increasing warming. Unlike the Ohio river basin, the other parts of MRB are projected to experience a decline in R95p from GWL1.5 to GWL2. This decrease is about 9% over Arkansas, lower Mississippi and centre Missouri region owing to additional 0.5°C warming. It is perceived widely that extremes precipitation will increase in the context of Paris agreement targets (Engelbrecht et al. 2015; James et al. 2017). Though, over the MRB an additional warming of 0.5°C in the MRB exhibits a decrease in extreme precipitation events over almost all the domain, particularly for R95p and CWD. The decrease in CWD is consistent to findings of Zhao et al. (2023). In fact, over the previously mentioned areas, extreme precipitation is projected to increase at GWL1.5 and will become more severe at GWL2. It is noteworthy that, under SSP2-4.5 (Figure S9) changing patterns of extreme precipitation indices are similar to changing patterns under SSP5-8.5, however substantial differences exist. For instance, under SSP2-4.5 (Figure S9), CWD decreases almost everywhere in the MRB vat GWL1.5 except lower Mississippi and Ohio region, compared to SSP5-8.5 where decreased CWD is observed only in the northern Missouri region at56 GWL1.5. Furthermore, with additional 0.5°C global warming, only the central Missouri region will experience decreasing R95p under SSP2-4.5 (Figure S9) which is different from what is observed under SSP5-8.5 (Figure 2) where in addition to central Missouri, Arkansas region and part of North MRB are also experiencing reduced R95p. Likewise, reduced frequency of CWD with additional warming is enhanced almost everywhere the MRB under SSP5-8.5 compared to SSP2-4.5 (Figure S9). Also, the intensity

TABLE 2 | Average percentage change in daily precipitation over sub-basins.

	SSP2-4.5		SS5-8.5	
Sub-basins	**1.5°C**	**2°C**	**1.5°C**	**2°C**
Ark	285%	292%	289%	290%
UM	179%	185%	182%	185%
LM	74%	77%	75%	76%
Ten	28%	29%	27%	30%
MO	210%	215%	212%	216%
Ohio	46%	48%	46%	49%
MRB	137%	141%	139%	141%

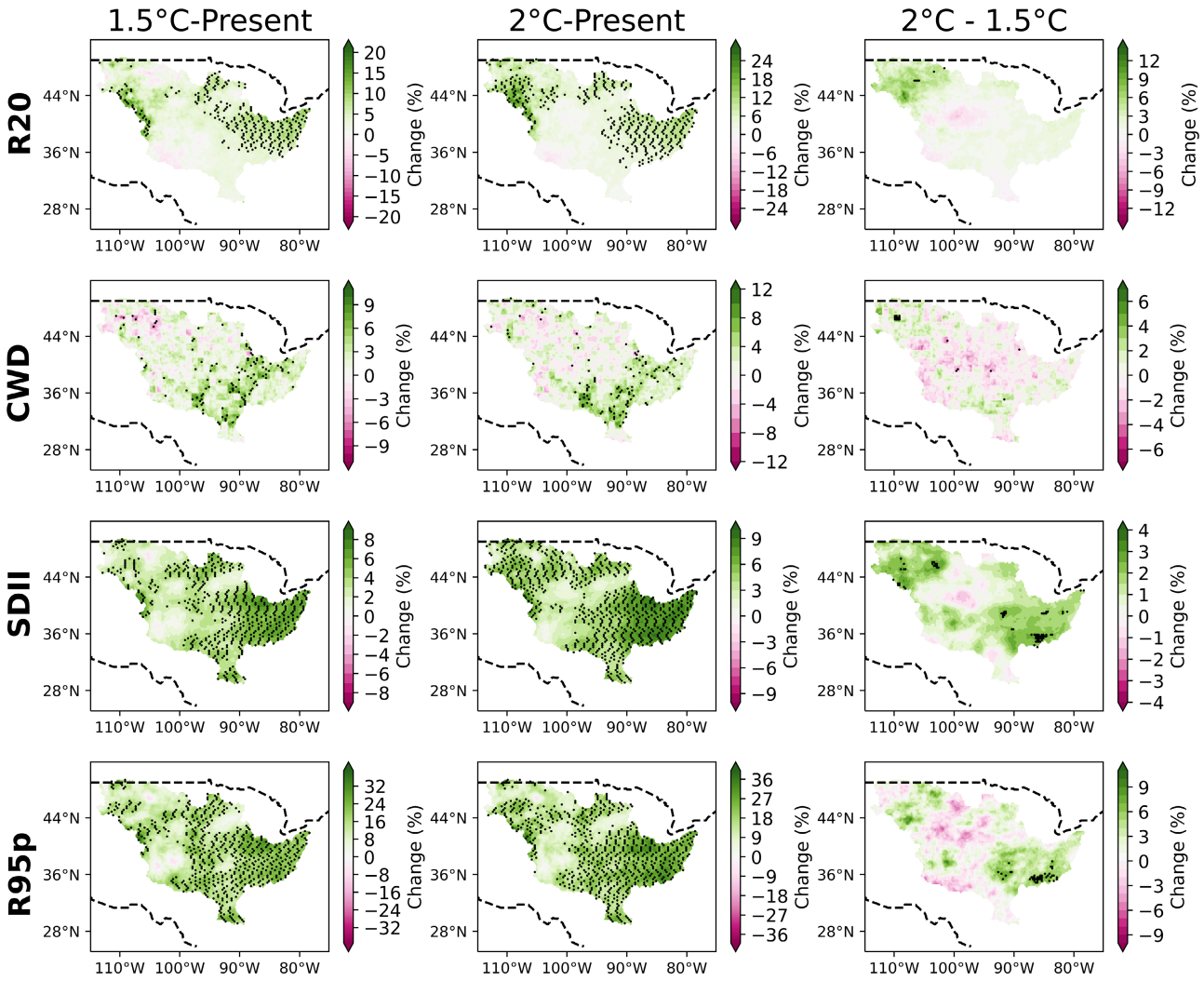

FIGURE 2 | Changes in extreme precipitation relative to the present day period (1971–2000) in 1.5°C (first column) and 2°C (second column) global warming for MME mean under SSP5-8.5. The MME means are computed as the average of all models for each global warming level. From top to bottom, the rows represent R20mm, CWD, SDII, and R95p, respectively. The third column represents the additional changes due to an additional 0.5°C warming (difference between 2°C and 1.5°C). The dots areas are statistically significant at 95% according to the student t-test. [Colour figure can be viewed at wileyonlinelibrary.com]

of SDII shows a greater reduction under SSP5-8.5 compared to SSP2-4.5 with additional 0.5°C warming. This demonstrates that increasing temperature is projected to affect hydrological cycle over the MRB such as enhanced water scarcity under SSP5-8.5 compared to SSP2-4.5, highlighting the sensitivity of extreme precipitation to emission scenario.

4.2 | Changes in Extreme Temperature

Over the Missouri region, the surface temperature increases on average by 1.95°C (2.6°C) at GWL1.5 (GWL2) under SSP2-4.5 over the MRB. This corresponds to an average increase of about 21% and 28% at GWL1.5 and GWL2, respectively. Similarly, under SSP5-8.5, the surface temperature on average increases by 1.9°C and 2.7°C at GWL1.5 and GWL2, corresponding to about 21% and 29%, respectively. An additional 0.5°C warming (from 1.5°C to 2°C) increases the surface temperature by 0.68°C (0.78°C), corresponding to about 35% (41%) temperature rise under SSP2-4.5 (SSP5-8.5) (not shown).

Under SSP5-8.5 (Figure 3), the mean changes of ETR in the MRB are about −0.83°C and −1.26°C at GWL1.5 and GWL2 respectively leading to additional decrease of 0.42°C with an additional 0.5°C climate warming. This implies a decreased ETR as the temperature goes up. The decreased ETR is associated with averages increased TNn by 3.02°C and 4.32°C, which dominates the mean changes in TXx which are 2.19°C and 3.05°C at GWL1.5 and GWL2, respectively. A dipole distribution characterises the spatial pattern of changes in ETR. Regionally, the ETR is expected to increase by 3°C–4°C (2°C–3°C) over the western part of the MRB encompassing Arkansas and Missouri Region at GWL2 (GWL1.5) leading to increased ETR by 0.9°C with additional 0.5°C warming. On the other hand, decreased ETR by 4°C (3°C) is observed over the Upper Mississippi, Ohio, Lower Mississippi and Tennessee Region at GWL2 (GWL1.5). This leads to a decreased ETR of about 1.6°C with additional 0.5°C warming. The changes of TNn exhibits an increased TNn over the entire MRB at both GWL1.5 and GWL2. At GWL1.5, the peak (4°C) of increased TNn is observed at the northern part of Upper Mississippi at GWL1.5. At GWL2, the peak (6°C) of increased TNn expands to cover the entire Upper

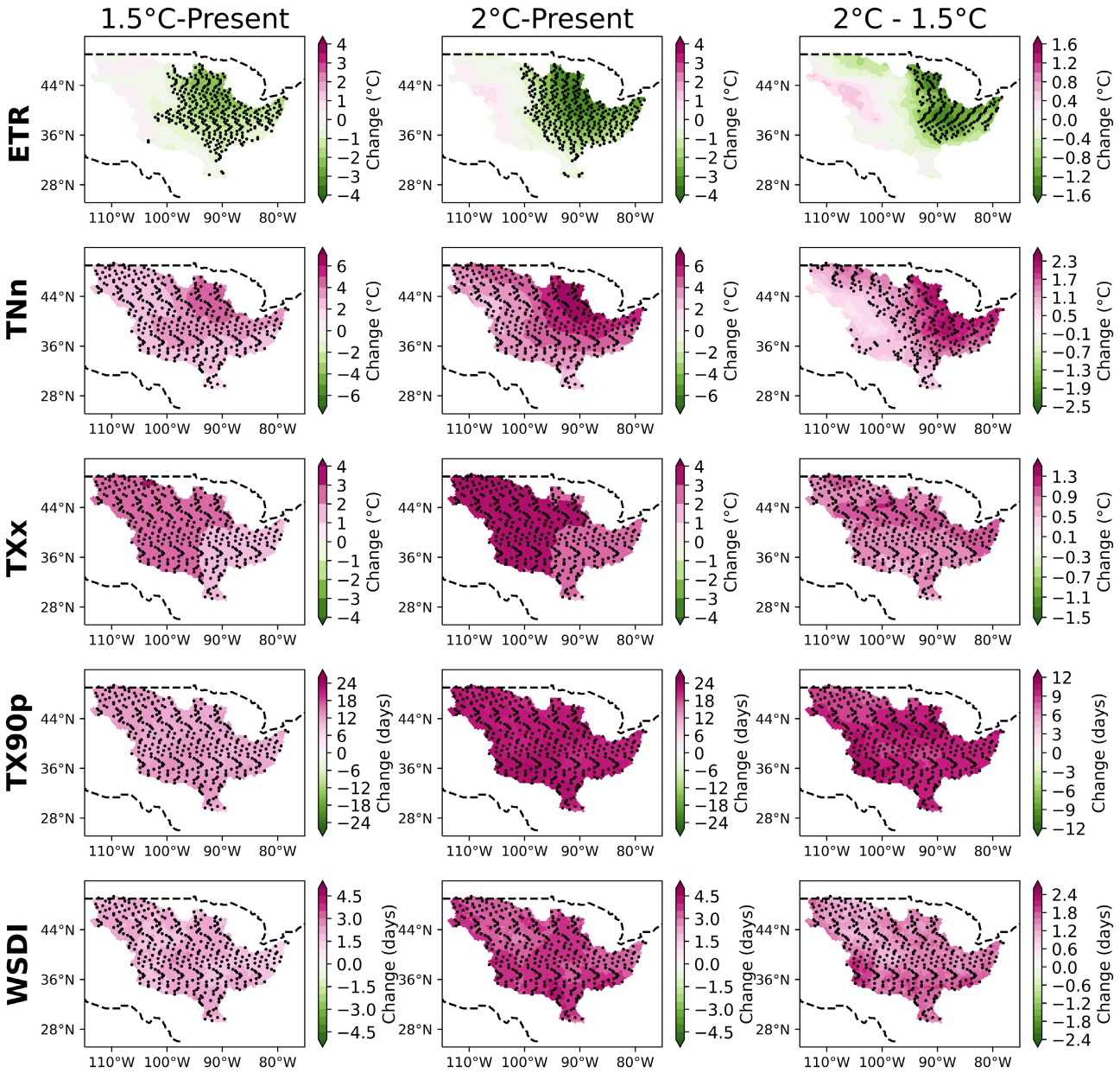

FIGURE 3 | Changes in extreme temperature relative to present day period (1971–2000) in 1.5°C (first column) and 2°C (second column) global warming for MME mean under SSP5-8.5. The MME means are computed as the average of all the models for each global warming level. From top to bottom, the rows represent ETR, TNn, TXx, TX90p, and WSDI respectively. The third column represents the additional changes due to an additional 0.5°C global warming (difference between 2°C and 1.5°C). The dots areas are statistically significant at 95% according to the student *t*-test. [Colour figure can be viewed at wileyonlinelibrary.com]

Mississippi and the Ohio region. This behaviour leads to enhanced increased TNn by 2.3°C within the Upper Mississippi and Ohio region with an additional 0.5°C warming. Like TNn, increased TXx is observed over the entire MRB at both GWL1.5 and GWL2, however there is a difference in their spatial variability. The peak of increased TXx by 3°C (4°C) occurs over the western part of MRB encompassing the Missouri, Arkansas and north Upper Mississippi region at GWL1.5 (GWL2). With increasing maximum temperature, warm days (TX90p) and warm spell duration (WSDI) are increasing also over the entire MRB at both GWL1.5 and GWL2, however with less spatial variability. The average increases of TX90p WSDI are about 12 days and 21 days at GWL1.5 and GWL2 respectively. As a result, TX90p increases by 9 days with an additional 0.5°C warming of the climate. Likewise, the WSDI increase by 2 days and 4 days at GWL1.5 and GWL2 respectively, leading to an increase by 1.5 days with additional 0.5°C warming. Similar behaviour is observed under SSP2-4.5 (Figure S10) regarding the spatial variability of the change in extreme temperatures indices, however differences in the magnitude of change are noticeable. For instance, under SSP2-4.5, TX90p increases by 21 days and 33 days at GWL1.5 and GWL2 respectively. Whilst under SSP5-8.5 the change in TX90p WSDI is about 12 days and 21 days at GWL1.5 and GWL2 respectively. Our results are consistent with Karmalkar and Bradley (2017) who found that temperature is increasing over the United States, but with great disparity in the magnitude of change across subregions. Our findings also align

with results from other parts of the world (Fotso-Kamga et al. 2023; Iyakaremye et al. 2020; You et al. 2022; Ngavom et al. 2024) where temperature related indices are projected to increase at GWL1.5 and more under GWL2. Overall, surface temperature over the MRB along with temperature indices are expected to increase at both global warming targets and scenarios. The enhancement of increased surface temperature and related indices under SSP5-8.5 shows their sensitivity to warming scenario.

4.3 | Regional Mean Changes

We start by showing in Figure 4 the mean change in extreme precipitation over the Mississippi sub-basin under SSP2-4.5 (Figure 4a) and SSP5-8.5 (Figure 4b). The most important changes are recorded for R95p both at GWL1.5 and GWL2 over the sub-basins and for the two scenarios. The minimum change in R95p is 12% over the Missouri river basin for both scenarios at GWL1.5. At GWL1.5, the change in R95p is almost similar and generally lower than 20%, with the exception being over the Ohio and Tennessee region which records about 23% for both SSP2-4.5 and SSP5-8.5. At GWL2, increased R95p generally exceeds 20% for both SSP2-4.5 and SSP5-8.5 except in the Missouri and Arkansas region where changes are about 18%. The observed increasing changes in R95p can exceed 30% for SSP5-8.5, particularly over the Ohio and Tennessee river basin, suggesting a greater occurrence of extreme rainfall over the entire MRB under both scenarios. This demonstrates the sensitivity of the changes in R95p over the MRB with climate scenarios. The changes in CWD are less than 5% over the sub-basins at SSP2-4.5 and SSP5-8.5, demonstrating substantial increased daily rainfall intensity at warmer climate. Similarly, the increased SDII and R20mm are also observed; however, they barely reach 8% at GWL1.5 and GWL2 at SSP2-4.5 and SSP5-8.5. Overall, a general increase in precipitation indices is observed over the entire MRB.

Figure 5 shows the changes in extreme temperatures over each sub-basin. Over the Missouri Arkansas River basin, the increase in TXx by 2.6°C is associated with increased TNn by 2.6°C at both GWL1.5 and GWL2 under SSP2-4.5, leading to the

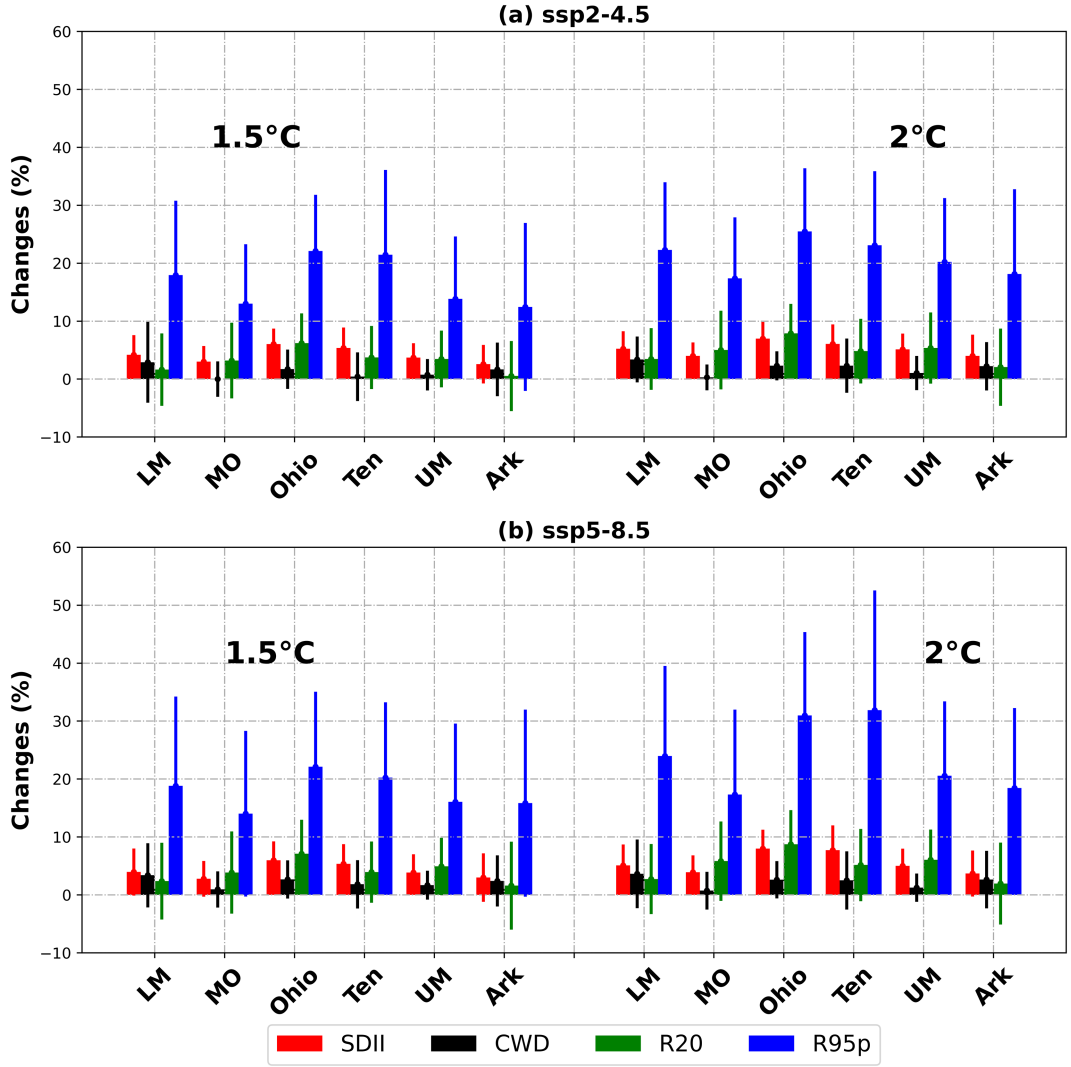

FIGURE 4 | The regional mean changes in extreme precipitation relative to present day period (1971–2000) at 1.5°C and 2°C global warming under (a) SSP2-4.5 and (b) SSP5-8.5. The sub-basins are denoted LM, MO, Ohio, Ten, UM, Ark for Lower Mississippi, Missouri River basin, Ohio river basin, Tennessee region, Upper Mississippi, and Arkansas respectively. The vertical lines over the bars indicate the range of standard deviations. [Colour figure can be viewed at wileyonlinelibrary.com]

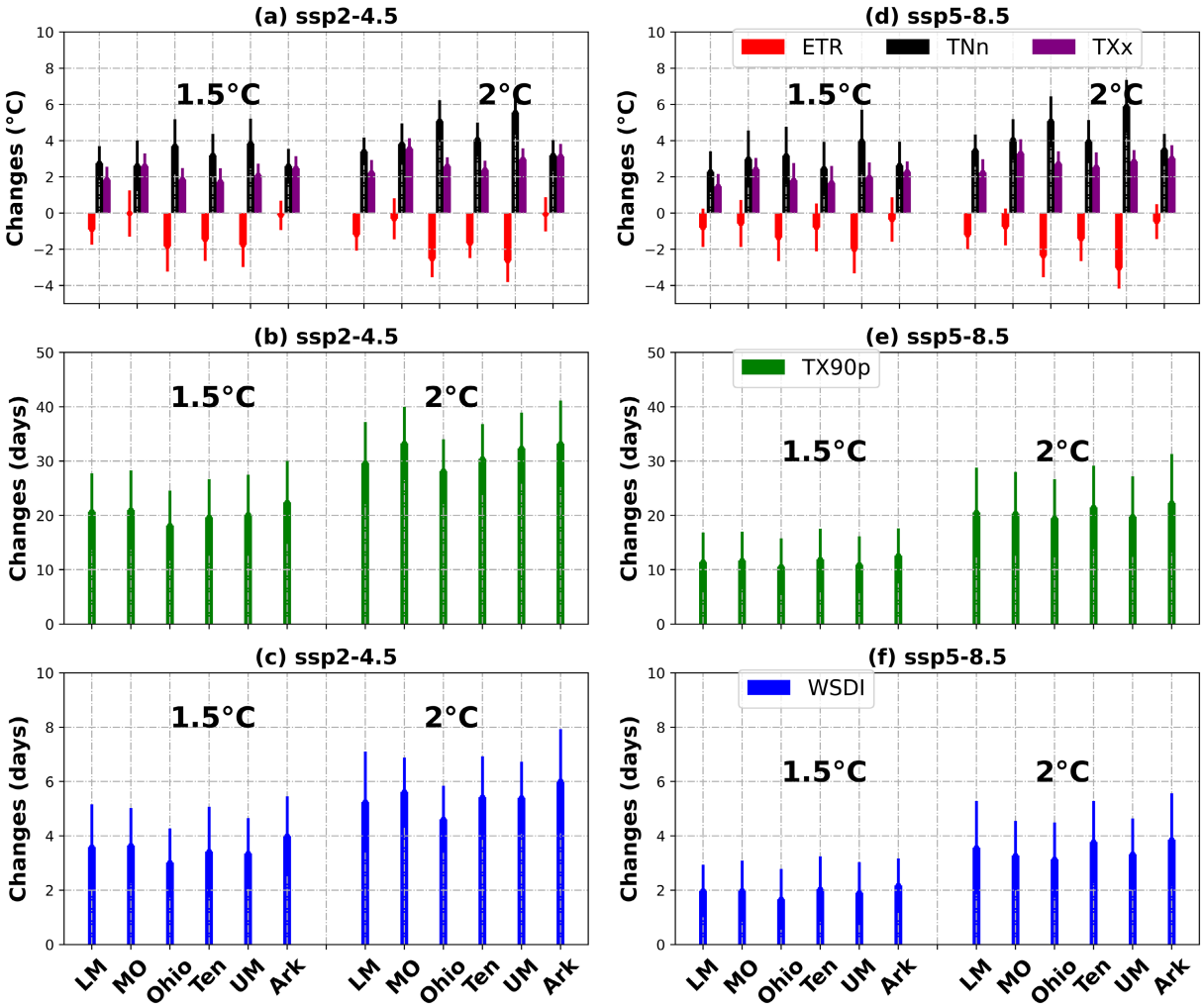

FIGURE 5 | As for Figure 3 but for extreme temperature. (a–d) ETR, TNn, TXx, (b–e) TX90p and (c–f) WSDI. [Colour figure can be viewed at wileyonlinelibrary.com]

cancellation of changes in ETR; however, at GWL2, a substantial increase in ETR by −0.3°C is associated with increased TNn, which dominates the increased TXx (a). Except for the above-mentioned regions, decreased ETR is observed over all the sub-regions due to increased TNn dominating the increased TXx in a warming climate. Under SSP2-4.5 (Figure 5a), the decreased ETR is more pronounced over Ohio, Tennessee, and Upper Mississippi at GWL1.5. This is justified by the increased TNn, which is twice the increased TXx in absolute values. Indeed, increased TNn (TXx) by 3.69°C (1.86°C), 3.19°C (1.73°C), and 3.84°C (2.08°C) leads to decreased ETR by 1.83°C, 1.46°C, and 1.75°C over Ohio, Tennessee, and Upper Mississippi, respectively. This behaviour is also observed at GWL2 but with larger values. In particular, the decreased ETR by 2.52°C and 2.63°C is associated with increased TNn by 5.08°C and 5.55°C, and increased TXx by 2.58°C and 2.97°C over Ohio and Upper Mississippi River basin, respectively. The changes in ETR, TXx, and TNn are similar under SSP5-8.5 (Figure 5b) as under SSP2-4.5 (Figure 5a); however, a substantial difference is observed within the Missouri and Arkansas region. Indeed, increased TNn is more pronounced under SSP5-8.5 compared to SSP2-4.5 in the aforementioned regions, both in GWL1.5 and GWL2; however, an unchanged ETR is observed. This led to a decreased ETR by 0.57°C (0.73°C) and 0.35°C (0.46°C) at GWL1.5 (GWL2) over the Missouri and Arkansas region, respectively. Under SSP2-4.5 (SSP5-8.5), the change on extremely warm days is about 20%/30% (10%/20%) at GWL1.5/GWL2. Indeed, at GWL2, the extremely warm days increase by 1.5 times more than at GWL1.5 under SSP2-4.5 (Figure 5c). This ratio doubles under SSP5-8.5 (Figure 5d). Similarly, the warm spell duration index (Figure 5e) increases by four (two) days at GWL1.5 and by six (four) days at GWL2 over the sub-basin under SSP2-4.5 (SSP5-8.5). This means that an additional warming of 0.5°C can double the number of extremely warm days and warm spell duration. This is a very relevant finding since a few changes in such extreme temperatures can have a harmful effect on crop growth (He and Chen 2022) with a devastating impact on crop yields (Vogel et al. 2019). Contrary to what is expected, the magnitude of changes in projected temperature-related indices (except for ETR, TXx, and TNn which exhibit almost the same magnitude) decreased from moderate (SSP2-4.5) to higher (SSP5-8.5) scenarios (Figure 5b–f). This is not consistent with findings in Ethiopia (Rettie et al. 2023b) and Central Africa (Ngavom et al. 2024), where the magnitude of changes in temperature indices consistently increases with the scenario.

The sensitivity of the results to forcing scenarios highlights the prominent impacts of human activities, particularly

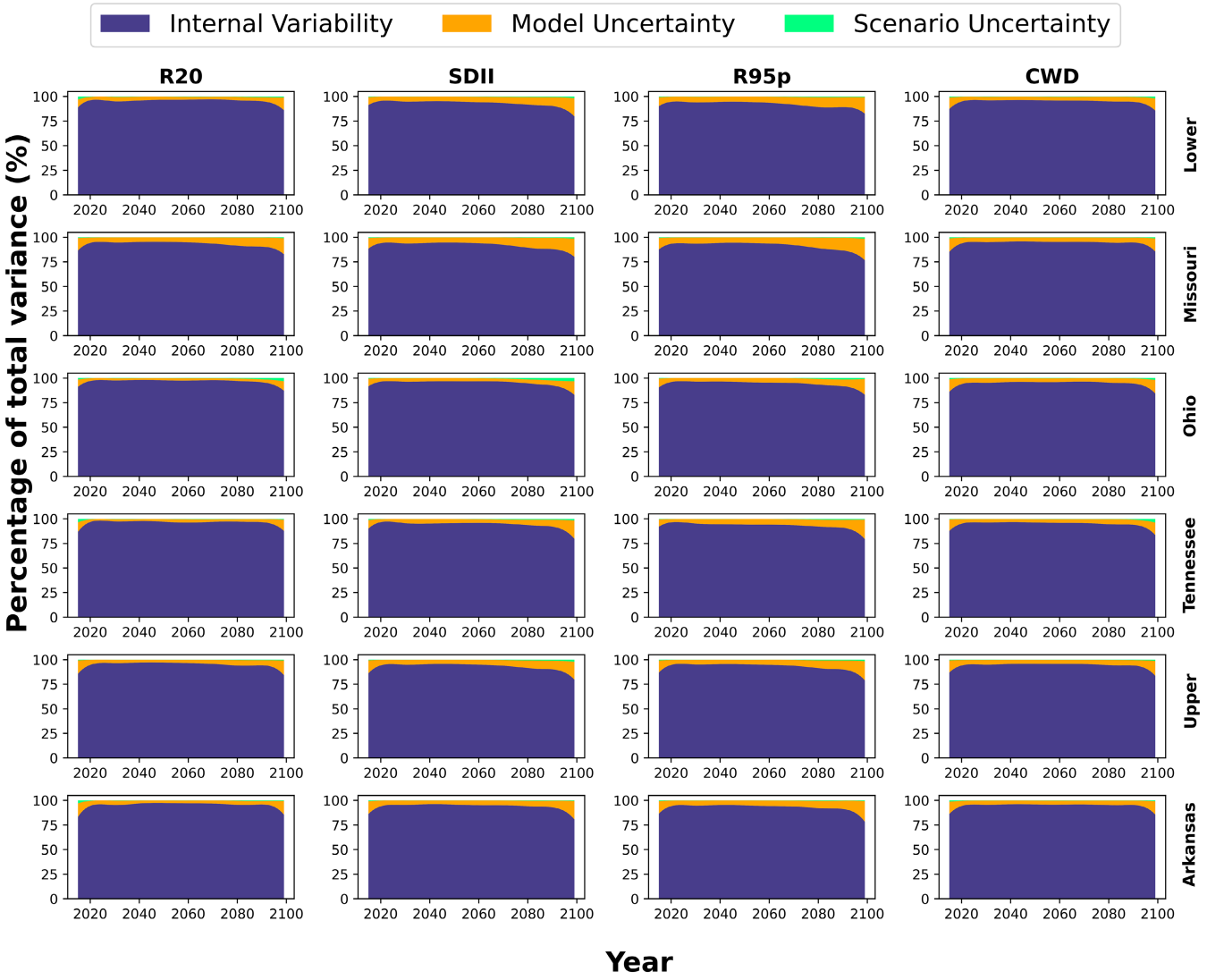

FIGURE 6 | Percentage shared of uncertainty for precipitation indices depicted by subregions for the period 2015–2099. [Colour figure can be viewed at wileyonlinelibrary.com]

greenhouse gas emissions leading to increased temperature resulting in increased ozone levels near the surface. This further leads to a significant impact on public health. For instance, increased ozone levels could potentially result to 10,000 of ozone-related deaths and illness in the United States by 2030 (Fann et al. 2014). Moreover, the increased temperatures, particularly extremely hot days (TX90p) is projected to cause premature deaths on projected population (Mills et al. 2014), additional annual mortality in Houston Texas (Marsha et al. 2016), and likely 10,000 additional annual deaths due to cardiovascular stress in the population aged 65 years and above in the Eastern United States (Limaye et al. 2018) in future emission scenarios. Conversely, the decreased ETR owing to the increased TNn dominating the increased TXx may be advantageous to infrastructure in the United States such as rail ways tracks which are less sensitive to thermal expansion if no other factors are considered (Martinich and Crimmins 2019). Prolonged occurrence of extremely hot days and warm spell duration may result in cracking soil, heat stress, and decreased water availability with consequences on crops yields and food security. Numerous findings have highlighted the environmental and economic impacts of precipitation related extreme indices over the United States in the coming decades. In addition to flooding, the increased SDII, extreme and heavy precipitation may result in infrastructure failure (Chinowsky et al. 2013; Wright et al. 2012; Chinowsky et al. 2019; Melvin et al. 2016), water quality (Boehlert et al. 2015), urban drainage problems, subsurface water overloading, surface erosion, nutrients transport, with consequence on crops heath and agriculture (Beach et al. 2015). Specifically, more than 10,000 bridges could be vulnerable to increased flooding due to projected increased SDII (Wright et al. 2012), and additional public expenditures ranging from $30 to $50 billion could arise if no mitigation policy is implemented to tackle the impact of increasing temperature on US agriculture during the period 2015–2100 (Beach et al. 2015). Overall, this research is anticipated to inform researchers, emergency managers, farmers, dam operators, insurance agents, lenders, and policy makers about creating strategies and mitigation plans to address the impacts of changing weather patterns on disaster recovery, conservation practises, farming operations, residential and commercial development, and regulations like zoning laws.

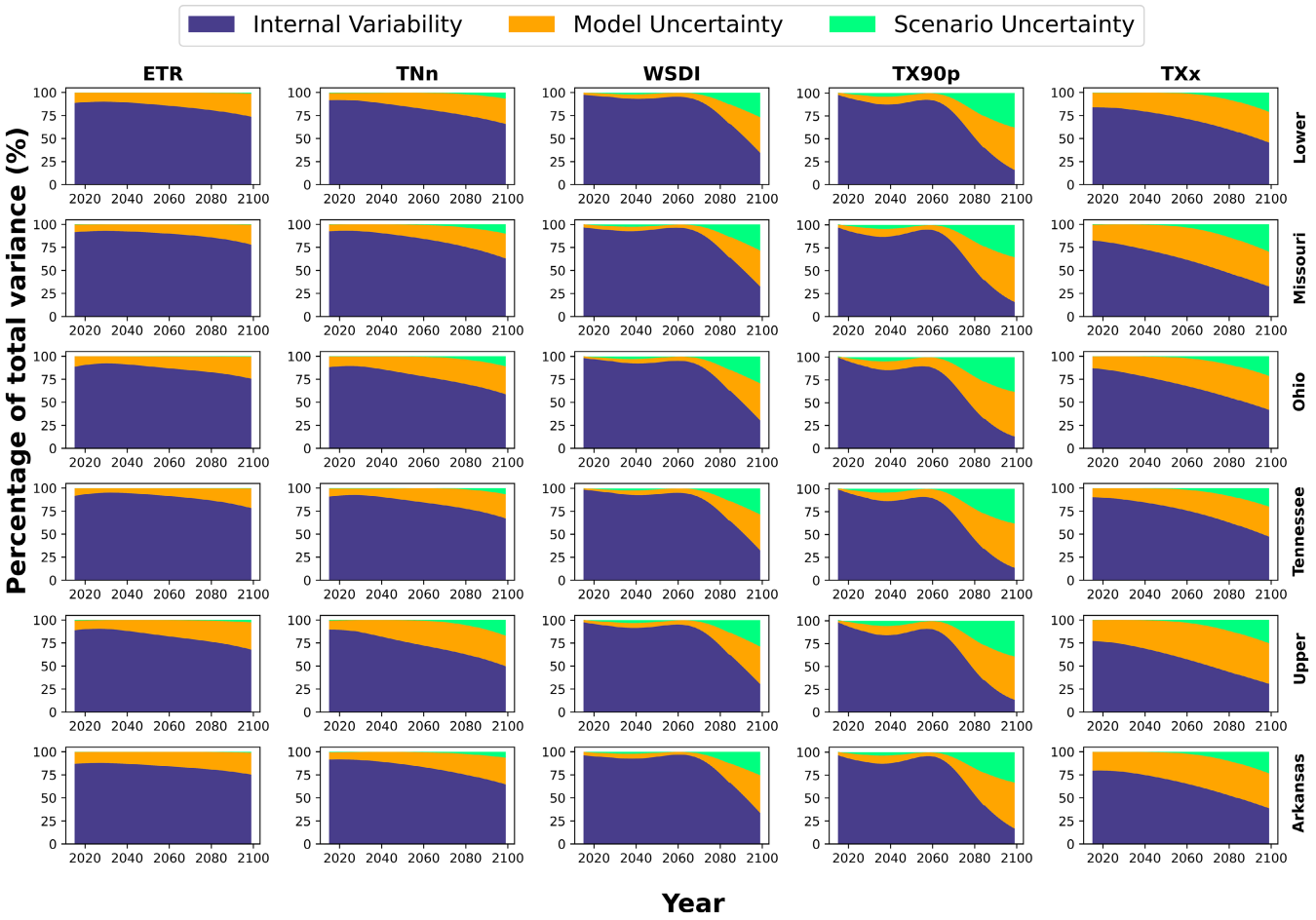

FIGURE 7 | Same as Figure 6 but for temperature indices. [Colour figure can be viewed at wileyonlinelibrary.com]

4.4 | Projection Uncertainty

Three sources of uncertainties in climate projections are assessed: (1) the uncertainty from climate sensitivity to external forcings (model or GCM uncertainty), (2) the natural climate variability (Internal variability) and (3) the uncertainty from different projection scenario (scenario uncertainty) (Hawkins and Sutton 2009, 2010; You et al. 2022; Rettie et al. 2023a). Figures 6 and 7 present the evolution of three sources of uncertainties for precipitations and temperature related indices respectively over each of the sub-basins. Precipitation-related indices indicate a general constant contribution of the internal variability (Figure 6) to total uncertainty throughout the time. The contribution of the internal variability accounts for about 75%, making it the largest contributor to total variance. These findings are largely consistent across different sub basins of the MRB. These results are also consistent with the findings of Hawkins and Sutton (2010) on a global scale who showed that internal variability is the main source of uncertainty in projected precipitation. Internal variability has been identified also as the prominent source of uncertainty in CDD and CWD in Ethiopia (Rettie et al. 2023b). The second largest contributor to total variance in the MRB, is the model uncertainty which accounts for about 20%–21% whereas the scenario uncertainty remains marginal across sub region.

Unlike precipitation related indices, uncertainties in temperature indices (Figure 7) vary considerably amongst indices and sub-basins. The contribution of internal variability (GCMs) to total variance is about 78%–80% (14%–20%) for ETR. These contributions from internal variability and GCMs are consistent over time across sub-regions, with contribution from SSPs being marginal. A slight decrease in internal variability is observed around 2060 before an increment just after 2080. Unlike ETR, TNn shows a decreased internal variability associated with a slight increased GCMs uncertainty from the beginning of the projected period (i.e., 2015) to the end (i.e., 2099) of the century. However, the uncertainty from SSPs remains marginal over time. For TNn, the contribution of internal variability to total variance ranges between 70% and 80% (18%–26%), whilst the uncertainty from SSPs lie between 1.5% and 4%. Decreased internal variability associated with increased GCMs and scenario uncertainty are observed around 2060 for WSDI, TX90p and TXx. These findings are largely consistent across all the subregions. Accordingly, the uncertainty from GCM (internal variability) accounts for about 3.5%–25.55% (73%–95%) at the beginning of projected period to about 42%–58% (13%–44%) by the end of the century. On the other hand, the uncertainty from SSPs account for about 0%–0.86% at the beginning of projected period to about 18%–38% by the end of the century for WSDI, TX90p and TXx. This is consistent with the findings of Karmalkar and Bradley (2017) who showed important contribution of scenario uncertainty to the total uncertainty in the projected temperature over the United States at the end of the 21st century.

4.5 | Robustness of the Projections

In this section, we quantify the signal to noise (S/N) ratio to depict the influence of uncertainties on projected extreme indices (Hawkins and Sutton 2009) and then evaluate the robustness of the projected changes in climate extremes (Hawkins and Sutton 2009, 2010). Figures 8 and 9 represent the S/N for precipitation and temperature related indices respectively for each of the sub-basin over the MRB. SDII and R95p exhibit an increasing S/N ratio for all the sub-basins whereas the number of heavy rainfall (R20mm) and the CWD show some variability over time. The S/N ratio is below unity despite an increase (Figure 8) from the beginning of the projected period to 2080 (a decrease with projection time is observed between 2080 and 2090 just before a slight increase at the end of the century) for most of the precipitation indices. This demonstrates that the magnitude of projected changes is smaller than the associated uncertainties. This also implies that uncertainties associated with projected changes make it less reliable and not well suited for decision making. Recent studies (Madakumbura et al. 2021; Zhang and Chen 2021; Birhan et al. 2021) showed that achieving reliable projection for precipitation has been a challenge due to its high uncertainty. One of the reasons of this challenge could be the inability of climate models in adequately simulating the El Niño–Southern Oscillation (ENSO-Korecha and Barnston 2007) which is one of the most important climate systems governing extreme precipitation across the MRB (Dommo et al. 2024) and the entire United States. Since most of the state-of-the-art global climate models fail to realistically simulate ENSO (Beobide-Arsuaga et al. 2021), the long-term projection of climate extreme might be affected as well. Therefore, the magnitude of the projected precipitation related extreme indices in this study might be considered with caution.

Largely consistent across the temperature-related extreme indices and for all the sub-basins (Figure 9), the S/N ratio increases with time except for the ETR which shows a decreasing trend. For almost all the sub-regions, the S/N ratio remains below unity. This demonstrates that the uncertainties dominate the magnitude of the changes over the MRB and hence the projected changes are not reliable. However, over the Upper Mississippi and Arkansas region, extremely warm days and warm spell duration reach its maximum (above unity) in mid-century (~2060) before a slight decay is observed until the end of the century. The peaks around 2060 could be related to the shifts in the contribution of uncertainties from different sources (i.e., SSPs, GCM and internal climate variability) (Figure 7).

5 | Discussion

Understanding changes in precipitation variability is important for a complete explanation of the hydrologic cycle response to global warming and its corresponding impacts. Future changes in precipitation and precipitation related indices are region dependent generally around the world. This study provides an assessment of model-projected precipitation and temperature extreme indices over the MRB at 1.5°C and 2°C global warming under SSP2-4.5 and SSP5-8.5. Although biases still persist, the bias corrected method shows significant improvement in simulating precipitation and temperature related indices. However, the corrected methods could be an additional source of uncertainties in projected climates extreme (Lafferty and Sriver 2023).

Our results also reveal that, under both scenarios (SSP2-4.5 and SSP5-8.5) significantly increased heavy precipitation (R20mm) is observed mainly over Ohio and northern Missouri region. This increased R20mm goes from up to 2.4 days at GWL1.5 to up to 4 days at GWL2 (not shown). Similarly, significantly increased SDII observed in Ohio region goes up to 2.4 mm/day probably due to increased daily precipitation (Figures S7 and S8). Contrary to R20mm, the changes in SDII are significant almost every here in the MRB, except in the northeastern part of the Arkansas region. Recent findings from Akinsanola et al. (2024) highlighted that under SSP5-8.5, the dynamics components of the moisture budget are the main factors contributing to increased daily precipitation over the US during the winter season. Largely consistent at both warming levels (GWL1.5 and GWL2) and both scenarios (SSP2-4.5 and SSP5-8.5), the significant increased SDII is accompanied by significant increased R95p and R20mm almost everywhere in the MRB, however, they are enhanced over the Lower Mississippi, Ohio and Tennessee region. Moreover, R95p exhibits high regional changes, reaching at least 20% of changes under SSP2-4.5 and SSP5-8.5 at GWL1.5 and GWL2. The combined effect of increases of heavy and intense rainfall can leads to strong flooding risks over lower Mississippi, Ohio and Tennessee region with considerable impacts on economies, delaying planting, crops damage and other flood related damages (Mantua et al. 2010; Changnon et al. 1997; Rosenzweig et al. 2002). Our results are consistent with findings from Akinsanola et al. (2020) who have found statistically robust increases in SDII and R20mm over the entire US, particularly during the winter season.

Regardless of the considered scenarios here (SSP2-4.5 or SSP5-8.5) temperature related indices (TNn, TXx, TX90p, WSDI) are projected to increase over the MRB. ETR exhibits a dipole spatial distribution with decreases over the Upper Mississippi, Ohio and Tennessee region and decreased over the western part of the domain encompassing Missouri, and Arkansas region. However, Figure 5 shows an average decreased ETR over all the sub-basins, resulting from increased TNn dominating the increased TXx. Under SSP2-4.5 (SSP5-8.5) an additional 0.5°C warming (i.e., from GWL1.5 to GWL2) increases in the changes of warm days and warm spell duration by 50% (100%). This implies a strong sensitivity of temperature changes with forcing scenario. However, it is worth noting that under SSP5-8.5, changes of TX90p and WSDI are smaller than under SSP2-4.5 both at GWL1.5 and GWL2 (Figure 5). For instance, TX90p increases by 20 days under SSP2-4.5 and by 10 days under SSP5-8.5 at GWL1.5. Similarly, WSDI increases by 30 days under SSP2-4.5 and by 20 days under SSP5-8.5 at GWL2. This can be explained by the threshold crossing time amongst the models considered in this study, rather than by a higher temperature under SSP2-4.5 compared to SSP5-8.5 as might be surmised. For instance, 1.5°C target is projected to be reached on average around 2031 with a standard deviation of 8.0 years under SSP2-4.5 and on average around 2027 with a standard deviation of 6.5 years under SSP5-8.5. Likewise, the 2°C target is projected to be reached on average around 2051 with a standard deviation of 15.0 years under SSP2-4.5 and on average around 2040 with

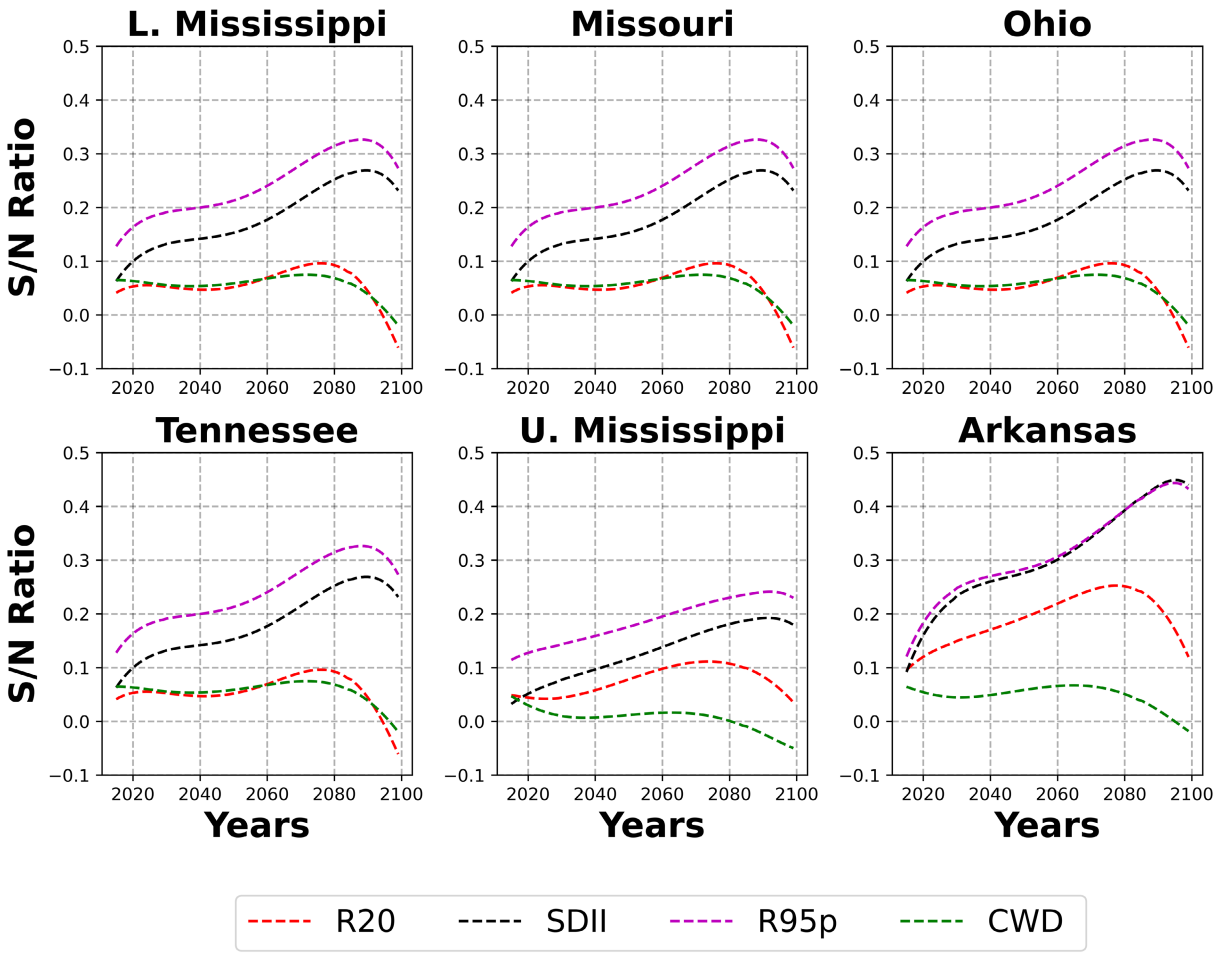

FIGURE 8 | Signal to noise ratio of the precipitation extreme indices depicted over each of the sub-basins. [Colour figure can be viewed at wileyonlinelibrary.com]

a standard deviation of 8.0 years under SSP5-8.5. This high inter-model variability on the threshold crossing time (see Table S2) under SSP2-4.5 could be the source of the large changes observed compared to SSP5-8.5.

The signal to noise ratio shows values below unity for temperature and precipitation related indices. This is contrary to what Karmalkar and Bradley (2017) found using a set 31 climate models with Representative Concentration Pathways (RCP), 4.5 and RCP8.5, to diagnose changes in mean temperature over the US. In fact, the projected precipitation and temperatures related extremes remain highly uncertain due to internal variability (Figures 6 and 7). In this work, we acknowledge that the use of only one realisation for every climate model is insufficient to capture the full effect on internal variability that plays a significant role in driving regional climate fluctuations over years or decades. Whilst this shortcoming is not expected to have a significant impact on our conclusions, we suggest that uncertainty estimated be treated as acceptable guidelines. The decomposition of uncertainty in this study highlights the predominance of internal variability from the beginning to the end of the century, follow by the model uncertainty and the substantial contribution of uncertainty from climate scenarios. This implies that for futures research, effort should be put into using a large set of climate models rather than climate scenarios. Because of the predominance of internal variability, we tested the performance of each of the models in simulating the precipitation and temperature for the period 1971–2000 with respect to the observational data. The models whose bias stand within the range of ±1.5 interannual standard deviation are identified as a better performing model. For the two models (CanESM5 and KACE-1-0-G) that stand out, the internal variability predominates (not shown). We hypothesise that even a perfect model's simulation will not necessarily prevent chaotic internal variability from arising (Mitchell et al. 2013; Tebaldi and Knutti 2007; Deser et al. 2012). Furthermore, a deep understanding of what drives climate and its variability on a local and regional scale is critical for future generations of climate models and future climate changes assessment. Climate extremes often arise due to internal variability and external forcings. However, internal variability can be large enough to overwhelm external forcings even on multidecadal time scale (Jain and Scaife 2022; Fischer et al. 2013). Some studies (Deser et al. 2012, 2014) highlighted that future precipitation and temperature projections over North America on local and regional scale could be subject to internal climate variability. For instance, Hong et al. (2025) highlight that the amplitude of El Niño Southern Oscillation (ENSO) and ENSO-induced atmospheric teleconnections are projected to be enhanced resulting to significant increases in US hydroclimate extreme events, with differences across region. Therefore, the ability of models to properly simulate the variability of some large scale atmospheric and oceanic circulation such as

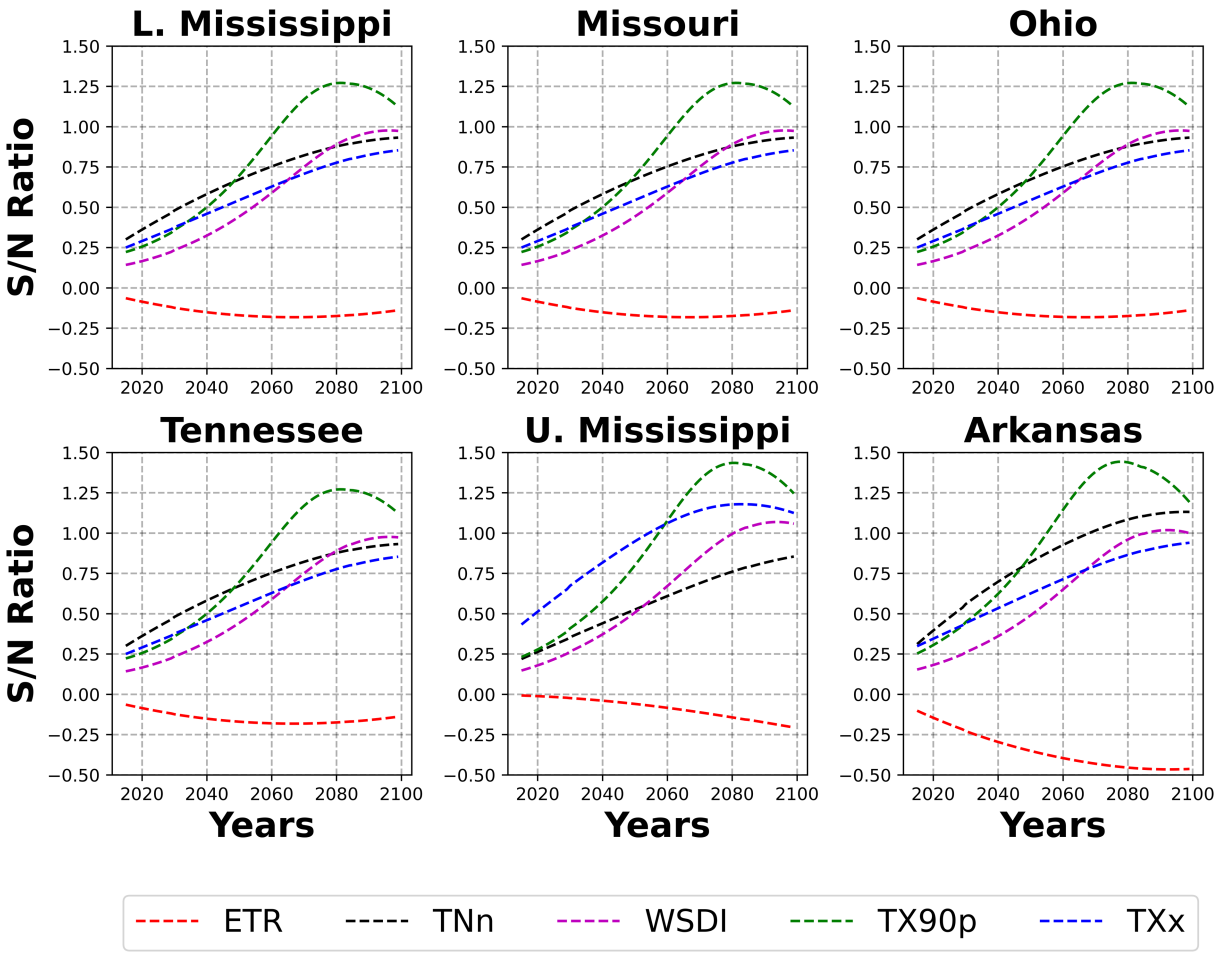

FIGURE 9 | Same as Figure 8 but for extreme temperature indices. [Colour figure can be viewed at wileyonlinelibrary.com]

ENSO, Pacific Decadal Oscillation (PDO) and North Atlantic Oscillation (NAO) are critical for the assessment of internal climate variability and future climate projections in order to meet the expectations of decision makers for accurate climate predictions.

6 | Conclusions

This study investigates the changes in precipitation and temperature related indices under SSP2-4.5 and SSP5-8.5 at 1.5°C and 2°C global warming using a set 12 high resolution CMIP6 models over the Mississippi river basin at its corresponding subregion. The spatial variability of the changes and the uncertainty associated with projected changes are investigated. The main findings can be itemised as follows:

1. Average daily precipitation is projected to increase under scenarios SSP2-4.5 and SSP5-8.5 at GWL1.5 and GWL2. However, changes at GWL2 exhibit a reduced daily precipitation compared to GWL1.5. This reduced daily rainfall is highly sensitive to warming scenario. This could result to more water scarcity at GWL2 under SSP5-8.5 compared to SSP2-4.5 over the Mississippi River Basin.
2. Regionally, the Missouri river basin, Arkansas region and part of Upper and lower Mississippi region are projected to experience major reduced daily rainfall at GWL2 under SSP5-8.5.
3. With an increase in climate warming, very heavy rainfall (R95p) associated with the increased simple daily intensity index (SDII) is projected to significantly increase everywhere in the Mississippi river basin compared to the period 1971–2000. Increased SDII and R95p are enhanced at GWL2 compared to GWL1.5 under both scenarios. Similarly, heavy precipitation (R20) is projected to significantly increase over the Ohio river basin and Northern Missouri at both warming level and projected scenario.
4. Temperature related indices (TNn, TXx, TX90p, WSDI) are projected to increase over the entire Mississippi River basin, except for ETR which exhibits otherwise. The decreased ETR results from the mean changes in TNn dominating the mean change in TXx as the temperature goes up. This implies in absolute value a rapid increase in TNn compared to TXx with global warming and warming scenario over the Mississippi River basin.
5. Internal variability dominates the uncertainty estimates for temperature and precipitation indices over the Mississippi river basin, with almost no contribution from scenarios.

Overall, this study provides insights on the precipitation and temperature behaviour over the Mississippi river basin, at 1.5°C

and 2°C global warming. Whilst we acknowledge that effort should be deployed in using a large set of climate models with many realisations, this work provides information on the potential upcoming water scarcity with consequences on agriculture and ecosystems.

Author Contributions

Atanas Dommo: conceptualization, investigation, writing – original draft, methodology, visualization, data curation, formal analysis, software. **Zachary Leasor:** writing – original draft. **Anthony Lupo:** supervision. **Sherry Hunt:** validation, project administration. **Noel Aloysius:** supervision, resources, funding acquisition.

Acknowledgements

USDA is an equal opportunity provider, employer, and lender. We are grateful to the two anonymous reviewers whose comments helped to improve the manuscript.

Conflicts of Interest

The authors declare no conflicts of interest.

Data Availability Statement

The data that support the findings of this study are openly available in copernicus climate Data Store at (https://cds.climate.copernicus.eu/datasets/projections-cmip6/).

References

Aerenson, T., C. Tebaldi, B. Sanderson, and J.-F. Lamarque. 2018. "Changes in a Suite of Indicators of Extreme Temperature and Precipitation Under 1.5 and 2 Degrees Warming." *Environmental Research Letters* 13, no. 3: 035009. https://doi.org/10.1088/1748-9326/aaafd6.

Akinsanola, A. A., Z. Chen, G. J. Kooperman, and V. Bobde. 2024. "Robust Future Intensification of Winter Precipitation Over the United States." *npj Climate and Atmospheric Science* 7, no. 1: 212. https://doi.org/10.1038/s41612-024-00761-8.

Akinsanola, A. A., G. J. Kooperman, A. G. Pendergrass, W. M. Hannah, and K. A. Reed. 2020. "Seasonal Representation of Extreme Precipitation Indices Over the United States in CMIP6 Present-Day Simulations." *Environmental Research Letters* 15, no. 9: 094003. https://doi.org/10.1088/1748-9326/ab92c1.

Anderson, B. T., D. J. Gianotti, and G. D. Salvucci. 2015. "Detectability of Historical Trends in Station-Based Precipitation Characteristics Over the Continental United States." *Journal of Geophysical Research: Atmospheres* 120, no. 10: 4842–4859. https://doi.org/10.1002/2014jd022960.

Anderson, B. T., J. Wang, G. Salvucci, S. Gopal, and S. Islam. 2010. "Observed Trends in Summertime Precipitation Over the Southwestern United States." *Journal of Climate* 23, no. 7: 1937–1944. https://doi.org/10.1175/2009jcli3317.1.

Beach, R. H., Y. Cai, A. Thomson, et al. 2015. "Climate Change Impacts on US Agriculture and Forestry: Benefits of Global Climate Stabilization." *Environmental Research Letters* 10, no. 9: 095004. https://doi.org/10.1088/1748-9326/10/9/095004.

Beobide-Arsuaga, G., T. Bayr, A. Reintges, and M. Latif. 2021. "Uncertainty of ENSO-Amplitude Projections in CMIP5 and CMIP6 Models." *Climate Dynamics* 56, no. 11–12: 3875–3888. https://doi.org/10.1007/s00382-021-05673-4.

Birhan, D. A., B. F. Zaitchik, K. T. Fantaye, B. S. Birhanu, G. A. Damot, and E. A. Tsegaye. 2021. "Observed and Projected Trends in Climate Extremes in a Tropical Highland Region: An Agroecosystem Perspective." *International Journal of Climatology* 42, no. 4: 2493–2513. https://doi.org/10.1002/joc.7378.

Bishop, D. A., A. P. Williams, R. Seager, et al. 2019. "Investigating the Causes of Increased Twentieth-Century Fall Precipitation Over the Southeastern United States." *Journal of Climate* 32, no. 2: 575–590. https://doi.org/10.1175/jcli-d-18-0244.1.

Boehlert, B., K. M. Strzepek, S. C. Chapra, et al. 2015. "Climate Change Impacts and Greenhouse Gas Mitigation Effects on U.S. Water Quality." *Journal of Advances in Modeling Earth Systems* 7, no. 3: 1326–1338. https://doi.org/10.1002/2014MS000400.

Cannon, A. J., S. R. Sobie, and T. Q. Murdock. 2015. "Bias Correction of GCM Precipitation by Quantile Mapping: How Well Do Methods Preserve Changes in Quantiles and Extremes?" *Journal of Climate* 28, no. 17: 6938–6959. https://doi.org/10.1175/jcli-d-14-00754.1.

Changnon, S. A., D. Changnon, E. R. Fosse, D. C. Hoganson, R. J. Roth, and J. M. Totsch. 1997. "Effects of Recent Weather Extremes on the Insurance Industry: Major Implications for the Atmospheric Sciences." *Bulletin of the American Meteorological Society* 78, no. 3: 425–436. https://doi.org/10.1175/1520-0477(1997)078<0425:EORWEO>2.0.CO;2.

Chinowsky, P., J. Helman, S. Gulati, J. Neumann, and J. Martinich. 2019. "Impacts of Climate Change on Operation of the US Rail Network." *Transport Policy* 75: 183–191. https://doi.org/10.1016/j.tranpol.2017.05.007.

Chinowsky, P. S., J. C. Price, and J. E. Neumann. 2013. "Assessment of Climate Change Adaptation Costs for the U.S. Road Network." *Global Environmental Change* 23, no. 4: 764–773. https://doi.org/10.1016/j.gloenvcha.2013.03.004.

Deser, C., R. Knutti, S. Solomon, and A. S. Phillips. 2012. "Communication of the Role of Natural Variability in Future North American Climate." *Nature Climate Change* 2, no. 11: 775–779. https://doi.org/10.1038/nclimate1562.

Deser, C., A. S. Phillips, M. A. Alexander, and B. V. Smoliak. 2014. "Projecting North American Climate Over the Next 50 Years: Uncertainty due to Internal Variability*." *Journal of Climate* 27, no. 6: 2271–2296. https://doi.org/10.1175/jcli-d-13-00451.1.

Dommo, A., N. Aloysius, A. Lupo, and S. Hunt. 2024. "Spatial and Temporal Analysis and Trends of Extreme Precipitation Over the Mississippi River Basin, USA During 1988–2017." *Journal of Hydrology: Regional Studies* 56: 101954. https://doi.org/10.1016/j.ejrh.2024.101954.

Eisenack, K., and M. Paschen. 2022. "Adapting Long-Lived Investments Under Climate Change Uncertainty." *Journal of Environmental Economics and Management* 116: 102743. https://doi.org/10.1016/j.jeem.2022.102743.

Engelbrecht, F., J. Adegoke, M.-J. Bopape, et al. 2015. "Projections of Rapidly Rising Surface Temperatures Over Africa Under Low Mitigation." *Environmental Research Letters* 10, no. 8: 085004. https://doi.org/10.1088/1748-9326/10/8/085004.

Eyring, V., S. Bony, G. A. Meehl, et al. 2016. "Overview of the Coupled Model Intercomparison Project Phase 6 (CMIP6) Experimental Design and Organization." *Geoscientific Model Development* 9, no. 5: 1937–1958. https://doi.org/10.5194/gmd-9-1937-2016.

Fann, N., C. G. Nolte, P. Dolwick, et al. 2014. "The Geographic Distribution and Economic Value of Climate Change-Related Ozone Health Impacts in the United States in 2030." *Journal of the air & Waste Management Association* 65, no. 5: 570–580.

Fischer, E. M., U. Beyerle, and R. Knutti. 2013. "Robust Spatially Aggregated Projections of Climate Extremes." *Nature Climate Change* 3, no. 12: 1033–1038. https://doi.org/10.1038/nclimate2051.

Foley, J. A., C. J. Kucharik, T. E. Twine, M. T. Coe, and S. D. Donner. 2004. "Land Use, Land Cover, and Climate Change Across the

Mississippi Basin: Impacts on Selected Land and Water Resources." In *Geophysical Monograph Series*, 249–261. American Geophysical Union.

Fotso-Kamga, G., T. C. Fotso-Nguemo, I. Diallo, et al. 2023. "Projected Changes in Extreme Precipitation and Temperature Events Over Central Africa From COSMO-CLM Simulations Under the Global Warming Level of 1.5°C and Above." *International Journal of Climatology* 43, no. 13: 6330–6351. https://doi.org/10.1002/joc.8208.

Gebrechorkos, S., J. Leyland, L. Slater, et al. 2023. "A High-Resolution Daily Global Dataset of Statistically Downscaled CMIP6 Models for Climate Impact Analyses." *Scientific Data* 10, no. 1: 611. https://doi.org/10.1038/s41597-023-02528-x.

Hansen, J., R. Ruedy, M. Sato, and K. Lo. 2010. "Global Surface Temperature Change." *Reviews of Geophysics* 48, no. 4. https://doi.org/10.1029/2010rg000345.

Hawkins, E., and R. Sutton. 2009. "The Potential to Narrow Uncertainty in Regional Climate Predictions." *Bulletin of the American Meteorological Society* 90, no. 8: 1095–1108. https://doi.org/10.1175/2009bams2607.1.

Hawkins, E., and R. Sutton. 2010. "The Potential to Narrow Uncertainty in Projections of Regional Precipitation Change." *Climate Dynamics* 37, no. 1–2: 407–418. https://doi.org/10.1007/s00382-010-0810-6.

He, X., and Z. Chen. 2022. "Weather, Cropland Expansion, and Deforestation in Ethiopia." *Journal of Environmental Economics and Management* 111: 102586. https://doi.org/10.1016/j.jeem.2021.102586.

Hong, J.-S., D. Kim, H. Lopez, S.-K. Lee, A. Mercer, and N. C. Johnson. 2025. "Projected Increase in ENSO-Induced US Winter Extreme Hydroclimate Events in SPEAR Large Ensemble Simulation." *npj Climate and Atmospheric Science* 8, no. 1: 84. https://doi.org/10.1038/s41612-025-00972-7.

Hunter, R. D., and R. K. Meentemeyer. 2005. "Climatologically Aided Mapping of Daily Precipitation and Temperature." *Journal of Applied Meteorology* 44, no. 10: 1501–1510. https://doi.org/10.1175/jam2295.1.

IPCC. 2022. *Climate Change 2022: Impacts, Adaptation, and Vulnerability. Contribution of Working Group II to the Sixth Assessment Report of the Intergovernmental Panel on Climate Change*, edited by H.-O. Pörtner, D. C. Roberts, M. Tignor, et al., 3056. Cambridge University Press. https://doi.org/10.1017/9781009325844.

Iyakaremye, V., G. Zeng, and G. Zhang. 2020. "Changes in Extreme Temperature Events Over Africa Under 1.5 and 2.0°C Global Warming Scenarios." *International Journal of Climatology* 41, no. 2: 1506–1524. https://doi.org/10.1002/joc.6868.

Jain, S., and A. A. Scaife. 2022. "How Extreme Could the Near Term Evolution of the Indian Summer Monsoon Rainfall Be?" *Environmental Research Letters* 17, no. 3: 034009. https://doi.org/10.1088/1748-9326/ac4655.

James, R., R. Washington, C. Schleussner, J. Rogelj, and D. Conway. 2017. "Characterizing Half-a-Degree Difference: A Review of Methods for Identifying Regional Climate Responses to Global Warming Targets." *Wiley Interdisciplinary Reviews: Climate Change* 8, no. 2: e457. https://doi.org/10.1002/wcc.457.

Jong, B.-T., T. L. Delworth, W. F. Cooke, K.-C. Tseng, and H. Murakami. 2023. "Increases in Extreme Precipitation Over the Northeast United States Using High-Resolution Climate Model Simulations." *npj Climate and Atmospheric Science* 6, no. 1: 18. https://doi.org/10.1038/s41612-023-00347-w.

Karmalkar, A. V., and R. S. Bradley. 2017. "Consequences of Global Warming of 1.5°C and 2°C for Regional Temperature and Precipitation Changes in the Contiguous United States." *PLoS One* 12, no. 1: e0168697. https://doi.org/10.1371/journal.pone.0168697.

Kharin, V. V., F. W. Zwiers, X. Zhang, and M. Wehner. 2013. "Changes in Temperature and Precipitation Extremes in the CMIP5 Ensemble." *Climatic Change* 119, no. 2: 345–357. https://doi.org/10.1007/s10584-013-0705-8.

Korecha, D., and A. G. Barnston. 2007. "Predictability of June–September Rainfall in Ethiopia." *Monthly Weather Review* 135, no. 2: 628–650. https://doi.org/10.1175/mwr3304.1.

Lafferty, D. C., and R. L. Sriver. 2023. *Downscaling and Bias-Correction Contribute Considerable Uncertainty to Local Climate Projections in CMIP6*. Authorea, Inc.

Limaye, V. S., J. Vargo, M. Harkey, T. Holloway, and J. A. Patz. 2018. "Climate Change and Heat-Related Excess Mortality in the Eastern USA." *EcoHealth* 15, no. 3: 485–496. https://doi.org/10.1007/s10393-018-1363-0.

Madakumbura, G. D., C. W. Thackeray, J. Norris, N. Goldenson, and A. Hall. 2021. "Anthropogenic Influence on Extreme Precipitation Over Global Land Areas Seen in Multiple Observational Datasets." *Nature Communications* 12, no. 1: 3944. https://doi.org/10.1038/s41467-021-24262-x.

Mantua, N., I. Tohver, and A. Hamlet. 2010. "Climate Change Impacts on Streamflow Extremes and Summertime Stream Temperature and Their Possible Consequences for Freshwater Salmon Habitat in Washington State." *Climatic Change* 102, no. 1–2: 187–223. https://doi.org/10.1007/s10584-010-9845-2.

Marsha, A., S. R. Sain, M. J. Heaton, A. J. Monaghan, and O. V. Wilhelmi. 2016. "Influences of Climatic and Population Changes on Heat-Related Mortality in Houston, Texas, USA." *Climatic Change* 146, no. 3–4: 471–485. https://doi.org/10.1007/s10584-016-1775-1.

Martinich, J., and A. Crimmins. 2019. "Climate Damages and Adaptation Potential Across Diverse Sectors of the United States." *Nature Climate Change* 9, no. 5: 397–404. https://doi.org/10.1038/s41558-019-0444-6.

Masson-Delmotte, V., P. Zhai, A. Pirani, et al. 2021. "IPCC, 2021: Climate Change 2021: The Physical Science Basis." In *Contribution of Working Group I to the Sixth Assessment Report of the Intergovernmental Panel on Climate Change*, 1–16. Cambridge University Press. https://www.ipcc.ch/report/ar6/wg1/downloads/report/IPCC_AR6_WGI_FrontMatter.pdf.

Maurer, E. P., H. G. Hidalgo, T. Das, M. D. Dettinger, and D. R. Cayan. 2010. "The Utility of Daily Large-Scale Climate Data in the Assessment of Climate Change Impacts on Daily Streamflow in California." *Hydrology and Earth System Sciences* 14, no. 6: 1125–1138. https://doi.org/10.5194/hess-14-1125-2010.

Meehl, G. A., C. Covey, T. Delworth, et al. 2007. "THE WCRP CMIP3 Multimodel Dataset: A New Era in Climate Change Research." *Bulletin of the American Meteorological Society* 88, no. 9: 1383–1394. https://doi.org/10.1175/bams-88-9-1383.

Melvin, A. M., P. Larsen, B. Boehlert, et al. 2016. "Climate Change Damages to Alaska Public Infrastructure and the Economics of Proactive Adaptation." *Proceedings of the National Academy of Sciences* 114, no. 2. https://doi.org/10.1073/pnas.1611056113.

Mills, D., J. Schwartz, M. Lee, et al. 2014. "Climate Change Impacts on Extreme Temperature Mortality in Select Metropolitan Areas in the United States." *Climatic Change* 131, no. 1: 83–95. https://doi.org/10.1007/s10584-014-1154-8.

Mitchell, D. M., P. W. Thorne, P. A. Stott, and L. J. Gray. 2013. "Revisiting the Controversial Issue of Tropical Tropospheric Temperature Trends." *Geophysical Research Letters* 40, no. 11: 2801–2806. https://doi.org/10.1002/grl.50465.

Muller, R. A., and R. J. Schaetzl. 1998. "Mississippi River: Encyclopedia Britannica." https://www.britannica.com/place/Mississippi-River.

Ngavom, Z., T. C. Fotso-Nguemo, D. A. Vondou, et al. 2024. "Projected Changes in Population Exposure to Extreme Precipitation Events Over Central Africa Under the Global Warming Levels of 1.5°C and 2°C: Insights From CMIP6 Simulations." *Modeling Earth Systems and*

Environment 10, no. 4: 5753–5769. https://doi.org/10.1007/s40808-024-02091-3.

O'Neill, B. C., C. Tebaldi, D. P. van Vuuren, et al. 2016. "The Scenario Model Intercomparison Project (Scenariomip) for CMIP6." *Geoscientific Model Development* 9, no. 9: 3461–3482. https://doi.org/10.5194/gmd-9-3461-2016.

Peterson, T. C., R. R. Heim Jr., R. Hirsch, et al. 2013. "Monitoring and Understanding Changes in Heat Waves, Cold Waves, Floods, and Droughts in the United States: State of Knowledge." *Bulletin of the American Meteorological Society* 94, no. 6: 821–834. https://doi.org/10.1175/bams-d-12-00066.1.

Pfahl, S., P. A. O'Gorman, and E. M. Fischer. 2017. "Understanding the Regional Pattern of Projected Future Changes in Extreme Precipitation." *Nature Climate Change* 7, no. 6: 423–427. https://doi.org/10.1038/nclimate3287.

Rettie, F. M., S. Gayler, T. K. D. Weber, K. Tesfaye, and T. Streck. 2023a. "Comprehensive Assessment of Climate Extremes in High-Resolution CMIP6 Projections for Ethiopia." *Frontiers in Environmental Science* 11: 1127265. https://doi.org/10.3389/fenvs.2023.1127265.

Rettie, F. M., S. Gayler, T. K. D. Weber, K. Tesfaye, and T. Streck. 2023b. "High-Resolution CMIP6 Climate Projections for Ethiopia Using the Gridded Statistical Downscaling Method." *Scientific Data* 10, no. 1: 442. https://doi.org/10.1038/s41597-023-02337-2.

Rogelj, J., G. Luderer, R. C. Pietzcker, et al. 2015. "Energy System Transformations for Limiting End-Of-Century Warming to Below 1.5°C." *Nature Climate Change* 5, no. 6: 519–527. https://doi.org/10.1038/nclimate2572.

Rosenzweig, C., F. N. Tubiello, R. Goldberg, E. Mills, and J. Bloomfield. 2002. "Increased Crop Damage in the US From Excess Precipitation Under Climate Change." *Global Environmental Change* 12, no. 3: 197–202. https://doi.org/10.1016/s0959-3780(02)00008-0.

Sheffield, J., G. Goteti, and E. F. Wood. 2006. "Development of a 50-Year High-Resolution Global Dataset of Meteorological Forcings for Land Surface Modeling." *Journal of Climate* 19, no. 13: 3088–3111. https://doi.org/10.1175/jcli3790.1.

Shi, C., Z.-H. Jiang, W.-L. Chen, and L. Li. 2018. "Changes in Temperature Extremes Over China Under 1.5°C and 2°C Global Warming Targets." *Advances in Climate Change Research* 9, no. 2: 120–129. https://doi.org/10.1016/j.accre.2017.11.003.

Smith, J. A., M. L. Baeck, Y. Su, G. A. Vecchi, and M. Liu. 2023. ""Strange Storms": Extreme Rainfall From the Remnants of Hurricane Ida (2021) in the Northeastern US." *Water Resources Research* 59, no. 3: e2022WR033934. https://doi.org/10.1029/2022WR033934.

Taylor, K. E., R. J. Stouffer, and G. A. Meehl. 2012. "An Overview of CMIP5 and the Experiment Design." *Bulletin of the American Meteorological Society* 93, no. 4: 485–498. https://doi.org/10.1175/bams-d-11-00094.1.

Tebaldi, C., and R. Knutti. 2007. "The Use of the Multi-Model Ensemble in Probabilistic Climate Projections." *Philosophical Transactions of the Royal Society A: Mathematical, Physical and Engineering Sciences* 365, no. 1857: 2053–2075. https://doi.org/10.1098/rsta.2007.2076.

Vautard, R., A. Gobiet, S. Sobolowski, et al. 2014. "The European Climate Under a 2 °C Global Warming." *Environmental Research Letters* 9, no. 3: 034006. https://doi.org/10.1088/1748-9326/9/3/034006.

Vogel, E., M. G. Donat, L. V. Alexander, et al. 2019. "The Effects of Climate Extremes on Global Agricultural Yields." *Environmental Research Letters* 14, no. 5: 054010. https://doi.org/10.1088/1748-9326/ab154b.

Werner, A. T., and A. J. Cannon. 2016. "Hydrologic Extremes—An Intercomparison of Multiple Gridded Statistical Downscaling Methods." *Hydrology and Earth System Sciences* 20, no. 4: 1483–1508. https://doi.org/10.5194/hess-20-1483-2016.

Wright, L., P. Chinowsky, K. Strzepek, et al. 2012. "Estimated Effects of Climate Change on Flood Vulnerability of U.S. Bridges." *Mitigation and Adaptation Strategies for Global Change* 17, no. 8: 939–955. https://doi.org/10.1007/s11027-011-9354-2.

Xie, S.-P., C. Deser, G. A. Vecchi, et al. 2015. "Towards Predictive Understanding of Regional Climate Change." *Nature Climate Change* 5, no. 10: 921–930. https://doi.org/10.1038/nclimate2689.

You, Q., Z. Jiang, X. Yue, et al. 2022. "Recent Frontiers of Climate Changes in East Asia at Global Warming of 1.5°C and 2°C." *npj Climate and Atmospheric Science* 5, no. 1: 80. https://doi.org/10.1038/s41612-022-00303-0.

Zhang, S., and J. Chen. 2021. "Uncertainty in Projection of Climate Extremes: A Comparison of CMIP5 and CMIP6." *Journal of Meteorological Research* 35, no. 4: 646–662. https://doi.org/10.1007/s13351-021-1012-3.

Zhao, J., T. Y. Gan, G. Zhang, and S. Zhang. 2023. "Projected Changes of Precipitation Extremes in North America Using CMIP6 Multi-Climate Model Ensembles." *Journal of Hydrology* 621: 129598. https://doi.org/10.1016/j.jhydrol.2023.129598.

Supporting Information

Additional supporting information can be found online in the Supporting Information section. **Data S1:** Supporting Information.